EFFECT OF APPROACH CHANNEL SHAPE ON THE FORMATION OF VORTICES AT SINGLE-HORIZONTAL INTAKES

A THESIS SUBMITTED TO
THE GRADUATE SCHOOL OF NATURAL AND APPLIED SCIENCES
OF
MIDDLE EAST TECHNICAL UNIVERSITY

BY

CAN METİN SÖNMEZ

IN PARTIAL FULFILLMENT OF THE REQUIREMENTS
FOR
THE DEGREE OF MASTER OF SCIENCE
IN
CIVIL ENGINEERING

SEPTEMBER 2019

Approval of the thesis:

EFFECT OF APPROACH CHANNEL SHAPE ON THE FORMATION OF VORTICES AT SINGLE-HORIZONTAL INTAKES

submitted by **CAN METİN SÖNMEZ** in partial fulfillment of the requirements for the degree of **Master of Science in Civil Engineering Department, Middle East Technical University** by,

Prof. Dr. Halil Kalıpçılar
Dean, Graduate School of **Natural and Applied Sciences**

Prof. Dr. Ahmet Türer
Head of Department, **Civil Engineering**

Prof. Dr. Mustafa Göğüş
Supervisor, **Civil Engineering, METU**

Examining Committee Members:

Prof. Dr. A. Burcu Altan Sakarya
Civil Engineering, METU

Prof. Dr. Mustafa Göğüş
Civil Engineering, METU

Prof. Dr. Mehmet Ali Kökpınar
Civil Engineering, TED University

Assist. Prof. Dr. Aslı Numanoğlu Genç
Civil Engineering, TED University

Assist. Prof. Dr. Elif Oğuz
Civil Engineering, METU

Date: 06.09.2019

I hereby declare that all information in this document has been obtained and presented in accordance with academic rules and ethical conduct. I also declare that, as required by these rules and conduct, I have fully cited and referenced all material and results that are not original to this work.

Name, Surname: Can Metin Sönmez

Signature:

ABSTRACT

EFFECT OF APPROACH CHANNEL SHAPE ON THE FORMATION OF VORTICES AT SINGLE-HORIZONTAL INTAKES

Sönmez, Can Metin
Master of Science, Civil Engineering
Supervisor: Prof. Dr. Mustafa Göğüş

September 2019, 76 pages

In an experimental setup of a water intake structure composed of a reservoir-pipe system, the formation of air-entraining vortices under symmetric flow conditions were investigated for different approach channel shapes. In the first set of the experiments the approach channel walls were kept parallel to each other and be perpendicular to the head-wall of the intake structure. In the following sets of the experiments these walls were located at different angles to the head-wall. A series of experiments were conducted on the model with varying approach channel shapes and a wide range of discharges to determine the critical submergences required for the formation of vortices. Consequently, the effect of the approach channel shape on the formation of air-entraining vortices were investigated. Experimental results show that critical submergence is mainly affected by Froude number and approach flow channel shapes. Moreover, a dimensionless equation, related with hydraulic and geometrical parameters, was obtained by using dimensional analysis for the critical submergence. Furthermore, empirical equations were derived to calculate critical submergence by using regression analysis. After that, simplified empirical equation was obtained by eliminating some of the dimensionless parameters. Furthermore, data obtained from the experiments and from the empirical equations are compared with each other's.

Keywords: Approach Channel Shape, Air-entraining Vortices, Critical Submergence, Single-horizontal Intakes

ÖZ

TEKİL – YATAY SU ALMA YAPILARINDA YAKLAŞIM KANALI ŞEKLİNİN VORTEKSLERİN OLUŞMASINA ETKİSİ

Sönmez, Can Metin
Yüksek Lisans, İnşaat Mühendisliği
Tez Danışmanı: Prof. Dr. Mustafa Göğüş

Eylül 2019, 76 sayfa

Bir rezervuar-boru sisteminden oluşan bir su alma yapısı deney düzeneğinde, simetrik akım şartları altında yaklaşım kanallarının farklı şekillerdeki durumlarında hava kabarcıklı vortekslerin oluşmaları incelendi. İlk başta yaklaşım kanalının yan duvarları birbirlerine paralel ve su alma yapısının alın duvarına ise dik olacak şekilde deney gurupları yapıldı. Daha sonraki deney gruplarında ise, bu duvarlar alın duvarına farklı açılarda tespit edildi. Model üzerinde geniş bir debi aralığında farklı şekillerde yerleştirilecek yaklaşım kanalları ile bir seri deney yapıldı ve her birisinde vortekslerin oluşması için gerekli olan su alma yapısının "kritik batıklık" değerleri tespit edildi. Neticede, yaklaşım kanalı şeklinin su alma yapısının önünde hava kabarcıklı vortex oluşumuna etkisi araştırıldı. Deney sonuçları neticesinde kritik batıklık değerinin genel olarak Froude sayısından ve yaklaşım kanalı şeklinden etkilendiği tespit edildi. Kirik batıklık değeri için gerekli hidrolik ve geometrik özellikler kullanılarak boyutsal analiz yapılıp boyutsuz bir denklem elde edilmiştir. Kritik batıklık değerini hesaplamak için regrasyon analizi yöntemi kullanılarak ampirik denklemler elde edilmiştir. Sonrasına bazı boyutsuz parametreler ampirik formüllerden elimine edilip basitleştirilmiş ampirik denklem elde edilmiştir. Sonrasında deneylerden elde edilen sonuçlar ile bahsi geçen ampirik denklemlerden elde edilen sonuçlar karşılaştırılmıştır.

Anahtar Kelimeler: Yaklaşım Kanalı Şekli, Hava Sürükleyici Girdaplar, Kritik Batıklık Derinliği, Tekil Su Alma Yapıları

To my family

ACKNOWLEDGEMENTS

I would like to thank Prof. Dr. Mustafa GÖĞÜŞ for his patience, kindness and perfect guidance. During my experimental research, I always benefit from his huge experience and knowledge. Consequently, he has created building blocks of this study.

I would like to thank my father Muharrem SÖNMEZ and mother İpek SÖNMEZ for their endless love and compassion.

I would like to thank my colleague and lovely friend Begüm KAYA for her continuous support and companionship.

I would like to thank research assistant Emre HASPOLAT and Serkan GÖKMENER for their help and advices.

I spent a lot of time at the Hydromechanics Laboratory to conduct the experimental setup and collect data. During this period, laboratory technicians made great contribution to the experimental setup. Therefore, I would like to thank laboratory technicians for their help and contributions.

TABLE OF CONTENTS

LIST OF TABLES

TABLES

LIST OF FIGURES

FIGURES

LIST OF SYMBOLS

SYMBOLS

a	Vertical distance between the bottom point of the intake and the base of the reservoir
2b	Side wall Clearance
b	Distance between the centerline of the intake pipe and one of the side walls
b1	Small side wall clearance for asymmetrical approach flow conditions
b2	Large side wall clearance for asymmetrical approach flow conditions
B	Distance between existing plexiglass side walls
c1	Regression variable
c2	Regression variable
c3	Regression variable
c4	Regression variable
c5	Regression variable
C_d	Discharge coefficient of the intake in a uniform canal flow
D_i	Intake diameter
Fr	Intake Froude number
g	Gravity acceleration
K	Viscous correction Factor
K_o	Intake Kolf number
L	Length of the approach channel
L_r	Model length scale ratio
N_v	Viscous parameter, ratio of Froude number to Reynolds number

N_Γ	Circulation number
Q_i	Intake discharge
r	Radius of spherical sink surface in a uniform canal flow
R	Correlation coefficient
Re	Intake Reynolds number
Re_R	Radial Reynolds number
Sc	Critical submergence measured from the summit point of horizontal intakes
Sc*	Critical submergence measured from the center of horizontal intakes
U_∞	Velocity of uniform canal flow at the upstream of intake
V_i	Average velocity of the flow at the intake pipe
W	Distance between the right and left approach channel side walls at the frontal face of the intake structure
We	Intake Weber number
θ	Angles between the approach channel side walls and the front face of the intake structure
Γ	Average circulation imposed to flow
ν	Kinematic viscosity of water
ρ	Density of the fluid
μ	Dynamic viscosity of the fluid
σ	Surface tension of the fluid
ψ	Representation of geometrical parameter for asymmetrical approach flow conditions

CHAPTER 1

INTRODUCTION

1.1. Introduction to Hydropower Plants and Intake Vortices

Water is the main life source for human beings. Water been primarily used to drink and irrigation. When humans established large societies, they have needed excessive electrical energy demand. When mankind realized the power of the water, they used it to produce electrical energy by constructing hydropower plants.

On the other hand, there are alternative energy production methods rather than hydropower generation, such as thermal power and nuclear power generation. However, these energy production methods have negative effects on environment. Thermal power plants pollute the air by burning fossil fuels. Nuclear power plants, producing radioactive waste, is a great threat to Mother Nature and humans. The destructive effects of Chernobyl tragedy are still in our minds. Contrary to thermal and nuclear power generation, hydropower is fueled by water, so it is a clean source of energy. It is, however, very significant that humans should use the water resources effectively and wisely since they are increasingly depleted.

The major structure of hydropower is hydroelectric dam. It converts the potential energy to kinetic energy. Then kinetic energy is converted to electrical energy by turbine and generators. Firstly, intake structure collects water from reservoir and then water falls down through penstocks. Finally, the water strikes and turns the blades of turbines and consequently, electrical energy is produced.

Proper design of intakes is needed in order to satisfy two interdependent factors; minimizing cost along with maximizing efficiency. If position of the intake is close to the bottom of the reservoir, there are two consequent troubles. Cost of construction will be increased and excessive sediment accumulation may probably occur into the intake structure. If position of the intake is close to the water surface, the design will be economical and there is no risk of sedimentation. On the other hand, formation of vortices will be observed in the case where intake location is closer to water surface. Thus, the intake position should be arranged in such a way that there is neither vortices nor sedimentation and the structure is economical.

1.2. Critical Submergence

Distance between the free surface and the intake can be known as submergence. There are some types of intakes in terms of flow direction. Horizontal intakes are generally used for dams. For horizontal intakes, critical submergence can be defined as vertical distance between the water surface and top point of the horizontal intake when air-entraining vortices on the free surface begin to from. Figure 1.1 shows the critical submergence of various intake structures. Critical submergence of intakes is usually denoted by Sc.

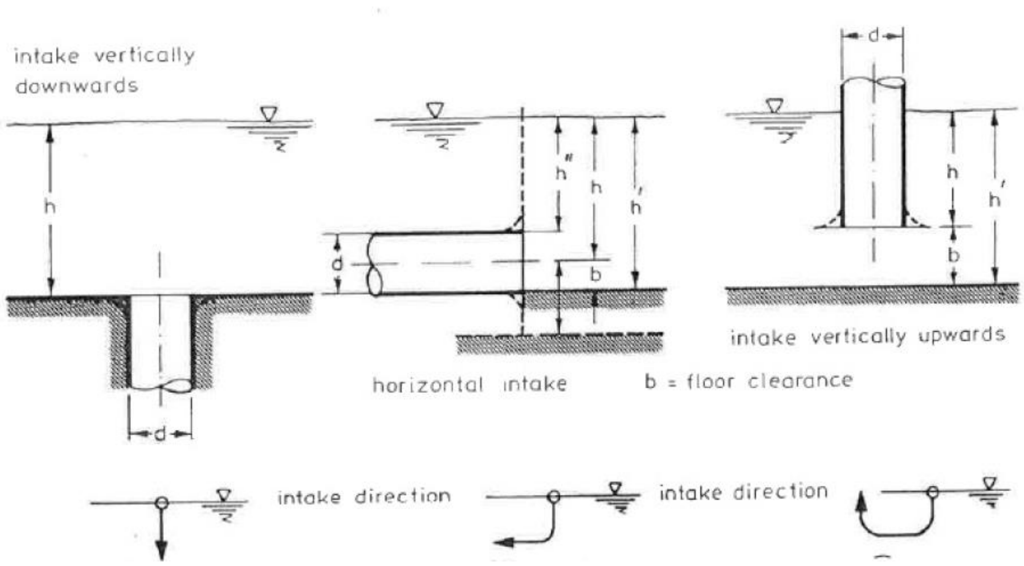

Figure 1.1 Critical Submergence of Various Intake Structures (Knauss, 1987)

Critical submergence should be satisfied in order to avoid vortices on the free surface since these vortices cause serious problems on the hydropower system such as;

significant reduction in flow capacity, increasing head loss of the system, decrease in efficiency, excessive cavitation and vibration problems in hydraulic machines.

1.3. Triggers of Vortex Formation on Free Surface

Many studies have been conducted in order to clarify the main reasons of vortex formation. The vortices can be formed by three basic reasons according to Durgin & Hecker (1978). Figure 1.2 shows these basic reasons of vortex formation, which are listed below;

a) Eccentric position of the intake relative to symmetrical approach flow

b) Shear layers due to high velocity gradient

c) Rotational wakes due to obstructions

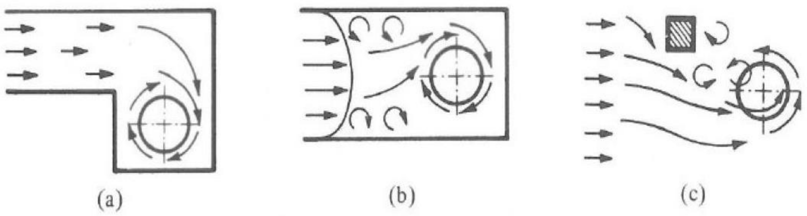

Figure 1.2 Basic Reasons of Vortex Formation (Durgin & Hecker, 1978)

1.4. Intake Types

Type of intakes has importance on critical submergence definition. They also affect classification of the air-entraining vortices. Intakes can be classified according to intake orientation and structural distinction, related with location of the intakes. Figure 1.3 shows the classification of intakes.

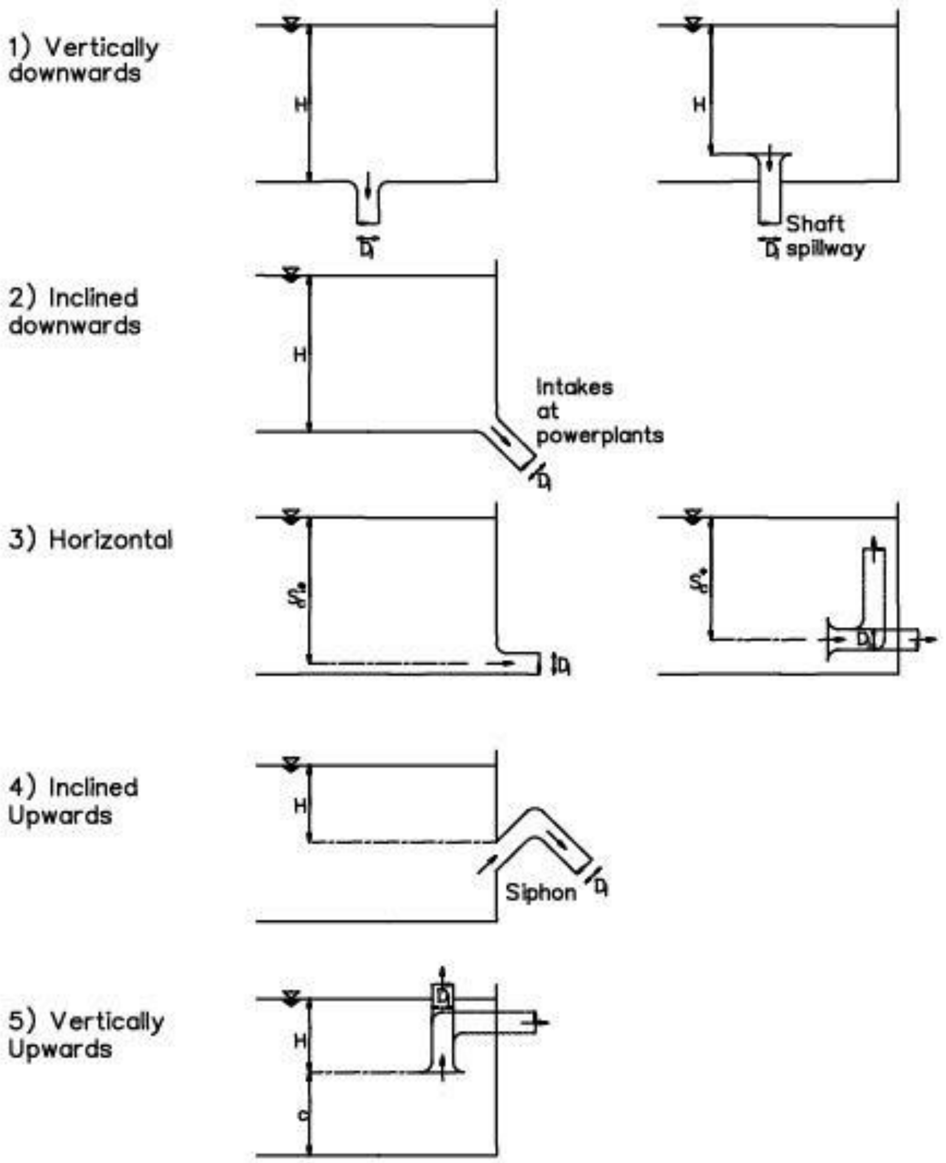

Figure 1.3 Classification of Intakes (Knauss 1987)

1.5. Vortex Types

Vortices can be classified in terms of their occurrence location, free water surface or subsurface vortices. Free water surface vortices result from swirling motion on the water surface. Since swirling occurs water surface, it contains air bubbles. On the other side, subsurface vortices, occur generally near the bottom and wall of the reservoir, induce swirling motion at the intake.

Another vortex classification is based on the strength of vortices. Visual method is used for this classification. Although visual method is obviously a subjective technique, it practically gives us important information about quality of design and performance of intakes. In literature, Knauss (1987) pointed out visual classification system, which has developed at the Alden Research Laboratory, ARL. He has explained vortex type with the words of “swirl, eddy, dimple and vortex tail” in terms of visual method. Formation of vortex tail begin with swirl motion of water. Then it is transformed into dimple by gaining strength. At the last stage, vortex tail occurs and it reaches to the intake. Figure 1.4 shows the phases of vortex tail formation.

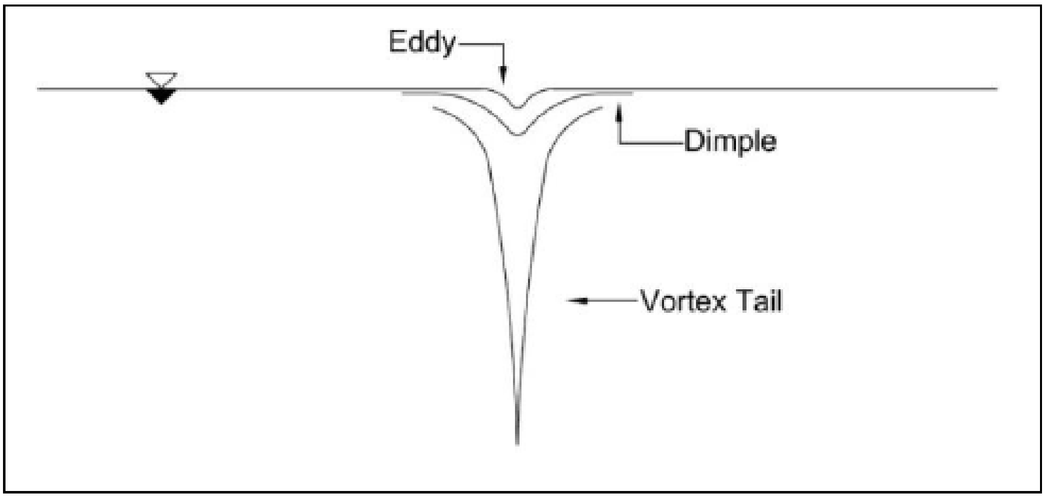

Figure 1.4 Phases of Vortex Tail Formation (Baykara, 2013)

Vortices can be classified into six steps during process of its formation. Figure 1.5 shows these six-vortex types.

1. Swirling motion stars at the free water surface. This can be seen as slight lines at water surface.

2. Swirling motion picks up speed and consequently surface dimples occurs, which start to appear with naked eyes.

3. Stronger dimple causes a tail, which stretches towards the intake. This tail does not contain air entrained bubbles. This phoneme can be observed if dye is put into water.

4. Whereas Type 4 vortex is stronger than Type 3 vortex, Type 4 vortex still does not contain air entrained bubble. However, it contains floating objects such as trash.

5. If the Type-4 vortex gains more strength, it captures air bubbles. Consequently, these air bubbles reach out the intake.

6. This type of vortex is the strongest one. Full air core is formed and its length starts from water surface to the entrance of intake. Therefore, it has conical shape with full of air and its appearance looks like a rope.

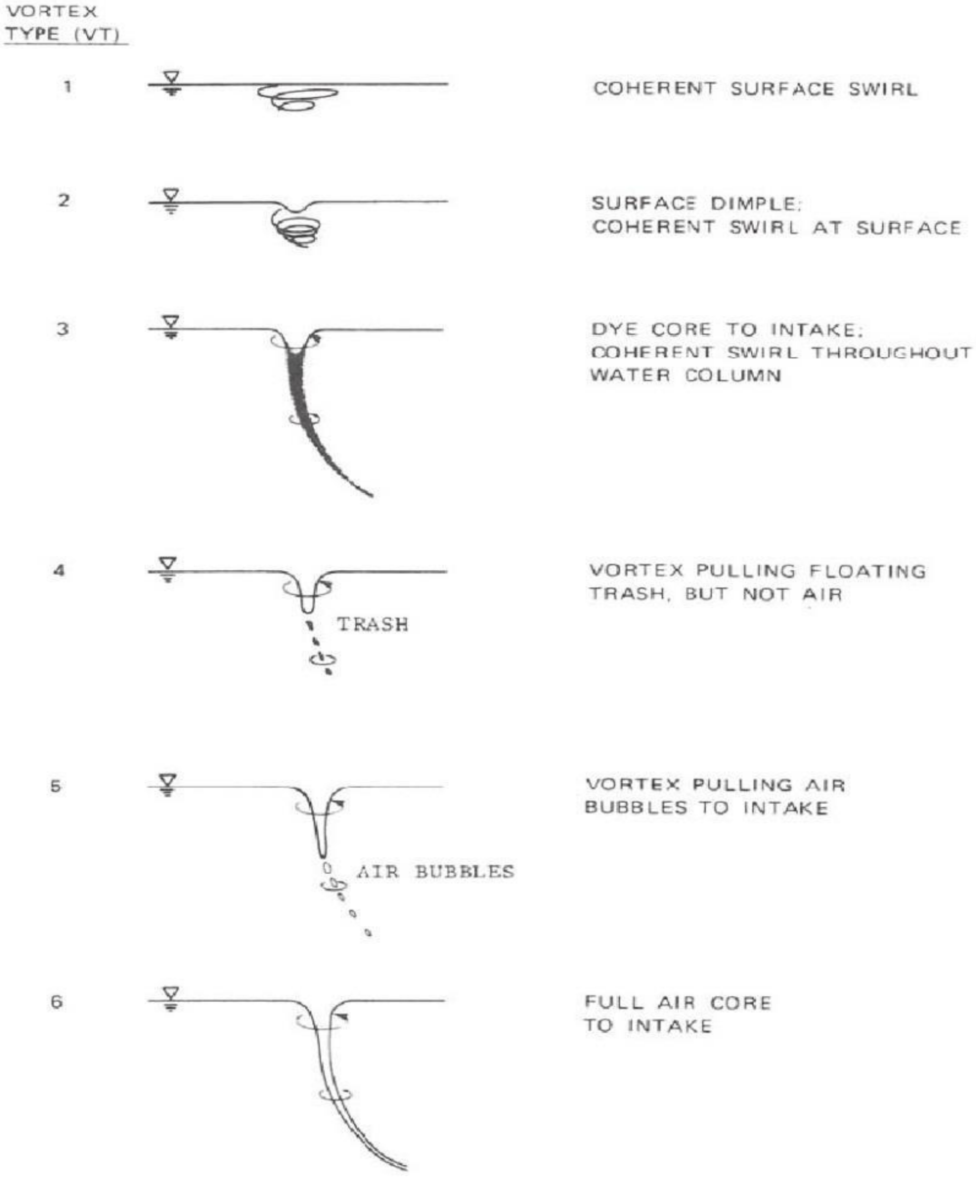

Figure 1.5 Vortex Types (Knauss 1987)

1.6. Scope of the Study and Outline of the Thesis

Aim of this study is to investigate critical submergence under the different approach channel shapes by experimental setup of water intake structure. The experimental setup mainly consists of a reservoir, horizontal intake pipes and approach channel walls. By adjusting various approach channel angles, different approach channel shapes are experimentally performed under symmetric flow conditions and wide range of discharges. These different approach channel shapes were applied to three different horizontal pipe diameters. Vortex Type 6 was used to determine critical submergence. Consequently, empirical equations of critical submergence were developed by using dimensional analysis for various symmetrical approach channel shapes.

Literature review related with vortex formation is presented in Chapter 2. After literature review, modelling of air entrained vortices and dimensionless parameters for the experimental model are demonstrated in Chapter 3. In Chapter 4, experimental setup and steps of performing the experiments are presented. Chapter 5 includes results of the experiments and their evaluation. Conclusions and recommendations are presented in Chapter 6.

CHAPTER 2

LITERATURE REVIEW

Analytical and numerical studies have been conducted in order to understand vortex formation and estimate submergence. However, these studies have resulted in complex equations for solution. Also, they use some assumptions in order to simplify the complexity. This simplification may ignore the unique nature of each hydraulic condition. Consequently, physical models are commonly preferred in order to deal with the complexity of vortex and real case problems.

Anwar (1967) performed investigations on vortices at low head intakes based on theoretical and experimental results for various types of flows. A tank, of which the top was closed, was used for the experiments. Answar pointed out that occurrence of vortices could be prevented by using floating raft on the water surface.

Answar (1968) studied prevention of vortices at intakes. In order to investigate how to prevent swirl and vortices formation, theoretical and experimental researches were conducted for various types of flows. It was claimed that position of intake plays an important role on vortex formation. In other words, inadequate submergence fundamentally causes vortices on the free water surface. Moreover, according to this study, occurrence of weak vortices or dimple waves were not dependent on radial Reynolds number, $Re_R=Q/(\nu S_c)$, if it was greater than $1x10^3$. Answar also indicated that increase in roughness of rigid boundary layer together with increase in radial Reynold number could prevent the vortex formation at intake. Using floating raft at the free water surface causes increase in roughness.

Gordon (1970) researched 29 existing hydroelectric intakes in order to generate design criteria about critical submergence. This study is one of the most adopted study in the literate. Gordon stated that there were 3 main factors, effecting formation of vortices.

- Velocity at the intake, Vi
- Submergence, S_c
- Intake diameter, D_i

As expected, Gordon (1970) developed the formulas by using these parameters. The formulas provide us to find critical submergence for symmetrical and asymmetrical flow conditions. Equations 2.1 and 2.2 show the relationship between critical submergence and Froude number for symmetrical and asymmetrical flow conditions, respectively.

$$\frac{S_c}{D_i} = 1.70\mathrm{Fr} \tag{2.1}$$

$$\frac{S_c}{D_i} = 2.27\mathrm{Fr} \tag{2.2}$$

In these equations, critical submergence and diameter of intake are indicated as "S_c" and "D_i", respectively and "Fr" represents Froude number $(= V_i/\sqrt{gD_i})$. Critical submergence is the vertical distance from free water surface to the summit point of the intake.

Reddy and Pickford (1972) observed formation of vortices at horizontal intakes in conventional pump sumps. They claimed that approach channel shape is important factor for the formation of vortices. Also, it was stated that Reynolds number, $Re=V_iD_i/\nu$, effects not significant due to the free water surface. Consequently, Reynolds number is eliminated from formulation of critical submergence. The relationship between critical submergence and Froude number is formulized as follows;

$$S_c/D_i = \mathrm{Fr} \tag{2.3}$$

If the vortex prevention devices are used, and

$$S_c/D_i = 1 + \mathrm{Fr} \tag{2.4}$$

If the vortex prevention devices are not used

Daggett and Keulegan (1974) searched surface tension and viscosity effect on formation of vortices. Different types of fluids, having different viscosity and surface tension, were used in the cylindrical tanks on the experiments. At the end of the experiments, they stated that after Reynolds number exceeds $5x10^5$, its effect on the formation of vortices can be ignored. Similarly, radial Reynolds number can be negligible when it is greater than $3x10^3$.

Zeigler (1976) conducted studies on the model of Grand Coulee Third Powerplant to investigate the effects of using trash rack, floating and submerged rafts on the formation of air entrained vortices. It was observed that intensity of vortices was decreased by using trash rack at the intake. Also, effects of using various grid size of trash rack on vortex formation was observed. Furthermore, in order to prevent vortices, floating and submerged rafts were used. Using these rafts decreased significantly occurrence of air-entrained vortices. However, it was observed that floating rafts were more efficient than submerged rafts to prevent air-entrained vortices.

Anwar et al. (1978) studied air entrained vortices in a horizontal intake. They stated that surface tension and viscosity were not affecting the formation of vortices under the conditions that the radial Reynolds number and Weber number, $We=\rho V_i^2 D_i/\sigma$, are greater than $3x10^4$ and $1x10^4$, respectively. They also concluded that critical submergence is not affected by bellmouth entrance. In other words, using bellmouth entry does not change the critical submergence compared to simple intake.

Jain et al. (1978) studied with two geometrically similar models of circular tanks to observe effects of surface tension, viscosity and model ratio on the formation of vortices. Each tank had horizontal intake and different fluid types in order to obtain different surface tension and viscosity values. It was found that both viscosity and surface tension does not affect the critical submergence depth when Reynolds number is within the range of $2.5x10^3<Re<6.5x10^3$ and Weber number is within the range of $1.2x10^2<We<3.4x10^4$. Moreover, it was mentioned that increase in viscosity of the fluid caused reduction in critical submergence due to reducing circulation. It was also stated that geometric similarity was satisfied as long as circulation parameter was kept constant. Therefore, there was only one factor caused to irregularities for Froude scaled models, which was different Reynolds number of the model and protype. A correction factor, K, was introduced to deal with those irregularities. Consequently, the relationship between critical submergence, Froude number, viscosity parameter and circulation number were formulized as;

$$K\frac{S_c}{D_i} = 5.6N_\Gamma^{0.42}Fr^{0.5} \qquad (2.5)$$

In that equation, K is the correction factor and N_v is a parameter function of viscosity, $N_v=g^{0.5}D_i^{1.5}/\nu$. N_Γ is the circulation number and equal to $N_\Gamma=\Gamma Sc/Q$ and Fr is the Froude number. This equation is valid in case of $5.3x10^2 \leq N_v$, $0.1875 \leq N_\Gamma \leq 1.95$ and $1.1 \leq Fr \leq 20$.

Gulliver and Rindels (1983) presented a graph, which shows critical submergence versus Froude number (Figure 2.1). This graph was generated to observe critical submergence from past data, belonging to Gordan (1970) and Reddy and Pickford (1972).

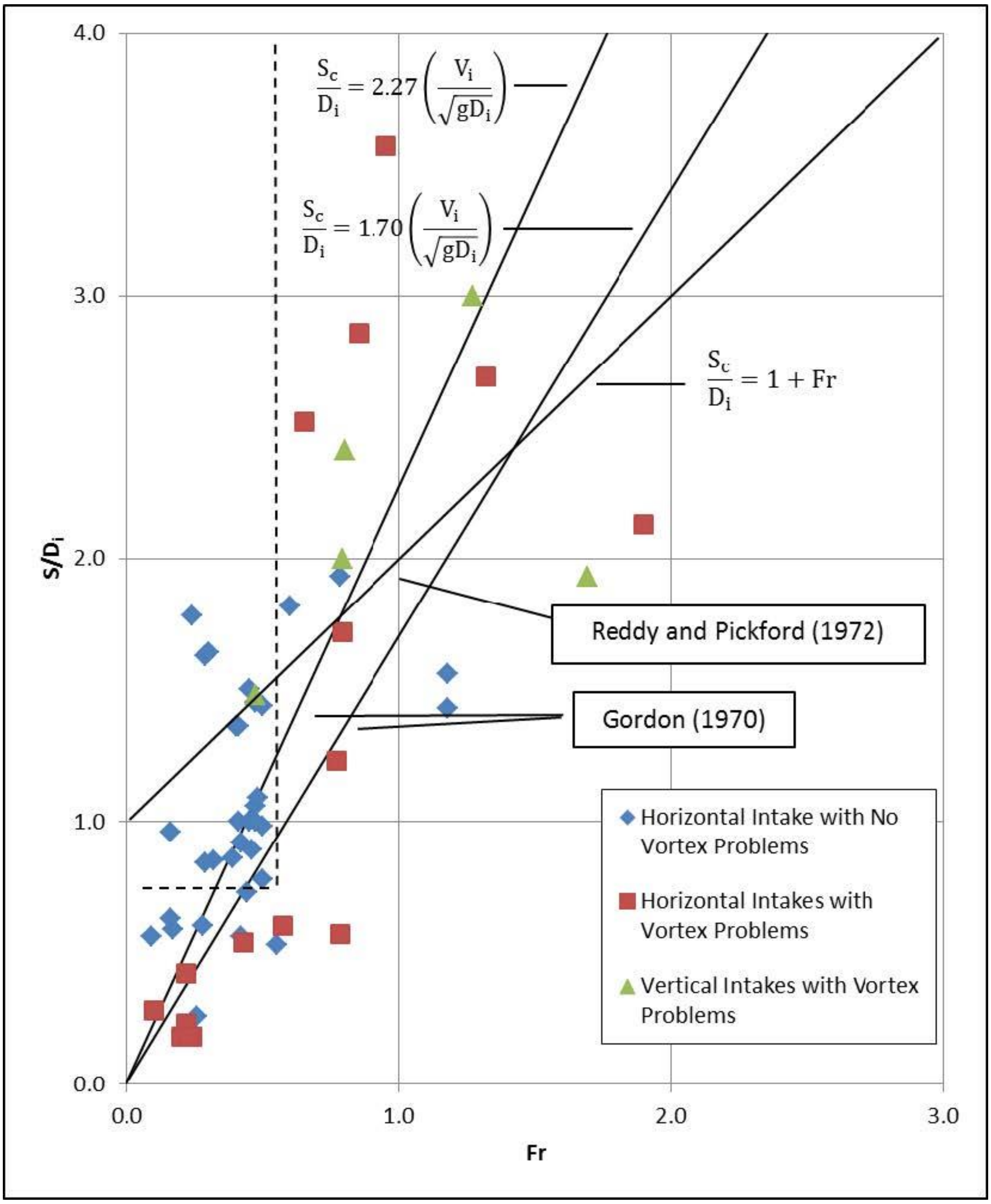

Figure 2.1 Past Data Related with Vortex Problem Gathered from Existing Intakes and Model Studies (Gulliver And Rindels, 1983)

Knauss (1987) studied critical submergence of air entrained vortices for some large intakes, belonging to power plants. He advised that critical submergence should be 1 to 1.5 times of the intake diameter. It was stated that the requirements for submergence can be found by the formula given in Figure 2.2.

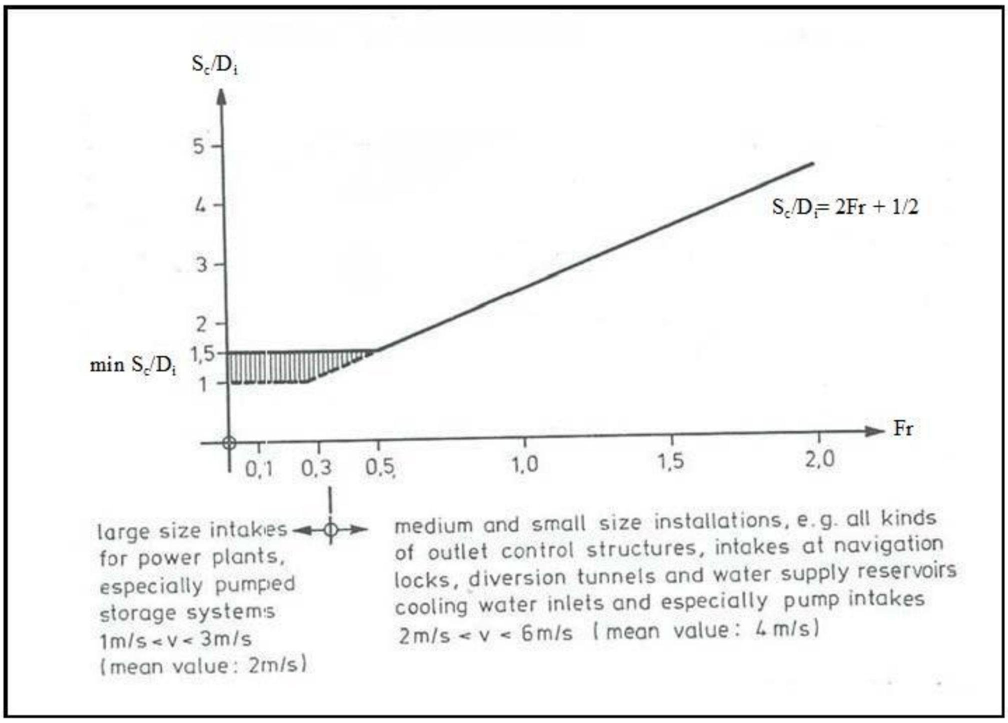

Figure 2.2 Recommended Submergence for Intakes with Proper Approach Flow Conditions, (Knauss, 1987)

Yıldırım and Kocabaş (1995) had experimentally and theoretically investigated critical submergence of intakes in uniform open canal flow. They had aimed that vortex problem was solved by using potential flow for the combination of point sink and uniform open canal flow, which is known as Rankine's half bodies. According to their theoretical and experimental results, critical submergence was equal to radius of imaginary spherical sink surface. In that case, half of the velocity in uniform canal flow is equal to radial velocity. As it can be seen in Figure 2.3, flow was thought to be superposition of uniform canal flow and point sink. They have found that there was slight difference between experimental and theoretical results.

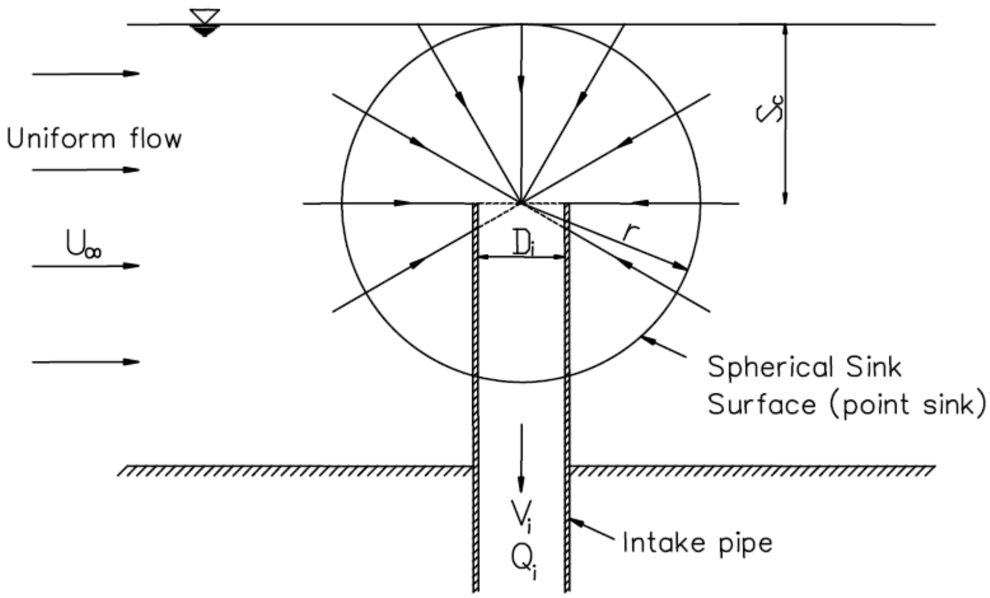

Figure 2.3 Uniform Flow , Point Sink and Critical Spherical Sink (Yıldırım and Kocabaş, 1995)

After establishing theoretically potential flow solution of the vortex problem, they derived a formula related with critical submergence as;

$$\frac{S_c}{D_i} = \frac{1}{2\sqrt{2}}\left(C_d \frac{V_i}{U_\infty}\right)^{1/2} \tag{2.6}$$

Where;

S_c, D_i, C_d, V_i and U_∞ are critical submergence, internal diameter of intake pipe, discharge coefficient, intake pipe velocity and velocity of uniform canal flow, respectively.

Jiming et al. (2000) performed experiments related with critical submergence of large-scaled models with double entrance pressure intakes. 1:30 scale model of Three Gorges Dam, which is the world's largest hydropower station in terms of installed capacity, was used in the experiments. Two empirical equations, related with critical submergence at double entrance intakes, were derived for symmetrical and non-symmetrical flow condition. Also, these equations were compared with Gordon's (1970) empirical equations.

Yıldırım et al. (2000) theoretically and experimentally investigated effects of flow boundary on critical submergence of an intake. Horizontal intake pipe, located at the dead-end wall of a flume was used in the experiments. It was stated that the deviation between theoretical solution, i.e. potential solution, and the analytical results increases when the distance between the intake pipes and dead-end wall is smaller than critical submergence.

Gürbüzdal (2009) experimentally studied formation of air-entrained vortices at horizontal intakes to show the effect of model scale on the phenomenon. In these experiments, four different intake pipes, placed in a large reservoir, were used. It was stated that model length scale ratio, side wall clearance ratio, Reynolds number and Froude number play an important role on critical submergence. It was also indicated that when ratio of side wall clearance to intake dimeter (b/D_i) is larger than 6, its effect on critical submergence is negligible. An empirical formula given below was derived to determine critical submergence considering the above-mentioned dimensionless parameters;

$$\frac{S_c}{D_i} = Fr^{0.865}\left(\frac{b}{D_i}\right)^{-0.565} Re^{0.0424} \tag{2.7}$$

Equation 2.7 is valid under the conditions of;

$0.51 \le Fr \le 4.03$, $1.597 \le b/D_i \le 5.147$ and $2.96x10^4 \le Re \le 2.89x10^5$

Yıldırım et al. (2009) conducted experiments with two vertical intakes to show the effect of intake size and location on critical submergence. From the results of the study it was concluded that critical submergence of dual intakes is higher than critical submergence of single intakes.

Taştan and Yıldırım (2010) investigated effects of dimensionless parameters and boundary friction on critical submergence of an intake. Experiments were performed in both no-circulation imposed cross flow and still water. It was stated that obtaining the critical submergence flow and geometrical conditions affect the limiting values of Froude number, Reynold number and Weber number.

Sarkardeh et al. (2010) experimentally investigated effects of intake head wall slope and trash rack in front of the intake on critical submergence as well as type and strength of intake vortices on a horizontal intake. The strength of voices was determined by an Acoustic Doppler Velocimeter device, which measures the tangential vortex velocity. Experiments were performed under condition of different intake head wall slopes, Z= 2:1, 3:1, 4:1 and vertical. Experiments were performed with and without trash rack. From the results of the experiments it was concluded that type and strength of vortices decreases if slope of the head wall increases. Also, it was stated that presence of trach rack reduces the strength and type of the vortices. Consequently, an empirical formula given below was derived to determine the critical submergence as a function of related dimensionless parameters;

For type 5, type 6 vortex and circulation number, $N_\Gamma > 0.016$;

$$\frac{\mathrm{S_c}}{\mathrm{D_i}} = 2.00\left(\frac{1}{Z}\right)^{0.008}(\mathrm{Fr})^{0.334}(\mathrm{T})^{0.369} \tag{2.8}$$

For type 3, type 4 vortex and circulation number, $N_\Gamma > 0.011$;

$$\frac{\mathrm{S_c}}{\mathrm{D_i}} = 2.43\left(\frac{1}{Z}\right)^{0.008}(\mathrm{Fr})^{0.334}(\mathrm{T})^{0.369} \tag{2.9}$$

Where Z is the head wall slope. T is the cross-sectional trash rack opening. Without a trash rack T is equal to 1.00. In their experiments, T is equal to 0.75 in case of presence of a trash rack.

Baykara (2013) conducted a series of experiments to prevent vortex formation at horizontal intakes by testing anti-vortex devices. In the experiments, six pipes of different diameters were used with various discharge range under symmetric approach flow conditions. Horizontal plates, located on top of the pipe, were used as an anti-vortex device and its effect on the formation of air-entrained vortices was investigated.

Consequently, some empirical equations were derived for specific range of dimensionless side wall clearance, $2b/D_i$, where b is the distance between the centerline of the intake pipe and one of the side walls, which was divided in three groups as maximum, minimum and intermediate values of S_c/D_i.

For maximum values of S_c/D_i, $1.33 \leq 2b/D_i \leq 4.00$,

$$\frac{S_c}{D_i} = Fr^{5.792} Re^{3.246} We^{-4.333} \left(\frac{2b}{D_i}\right)^{-3.489} \tag{2.10}$$

For minimum values of S_c/D_i, $2.00 \leq 2b/D_i \leq 8.00$,

$$\frac{S_c}{D_i} = Fr^{0.039} Re^{-0.357} We^{-0.425} \left(\frac{2b}{D_i}\right)^{-0.602} \tag{2.11}$$

For intermediate values of S_c/D_i, $3.33 \leq 2b/D_i \leq 12.00$,

$$\frac{S_c}{D_i} = Fr^{0.336} Re^{-0.229} We^{0.401} \left(\frac{2b}{D_i}\right)^{-0.261} \tag{2.12}$$

Taştan and Yıldırım (2014) investigated the effects of Froude, Reynolds and Weber numbers on formation of air entrained vortices by using a semi-theoretical approach. It was stated that S_c/D_i ratio can be modeled in case of only kinematic similarity is satisfied. Flow and geometrical properties can be ignored if S_c/D_i ratio is identical for intakes that have velocity ratios at the intake and critical spherical sink surface are the same.

Zaloğlu (2014) experimentally investigated effects of symmetrical and asymmetrical approach flow conditions on formation of air entrained vortices at water surface. Various symmetrical and asymmetrical approach flow conditions were created by help of adjustable lateral walls, made of plexiglass. The experiments were performed for a wide range of discharges and different pipe diameters, 25.0 cm, 19.4 cm and 14.4 cm. Consequently, after analyzing the results of the experiments, some empirical equations were derived and their results were compared with those of existing studies in the literature.

Haspolat (2015) conducted a series of experiments related with formation of air-entrained vortices in a model, composed of a reservoir and horizontal intake, in order to estimate critical submergence. The experiments were performed under symmetrical and asymmetrical approach flow conditions by using adjustable side walls. The similar experiments were repeated with four different pipe diameters for a wide range of discharges. Also, floating rafts with various dimensions on the water surface were used as anti-vortex devices in order to prevent formation of vortices. Consequently, empirical equations were derived considering Sc/D_i and other related flow and geometric parameters;

For symmetrical approach flow conditions, Equation 2.16 was derived with a correlation coefficient of R^2=0.966;

$$\frac{S_c}{D_i} = Fr^{0.193} Re^{-0.331} We^{0.544} \left(\frac{2b}{D_i}\right)^{-0.241} \tag{2.13}$$

Where 2b is the side wall clearance.

For asymmetrical approach flow conditions, Equation 2.17 was derived with a correlation coefficient of R^2=0.949;

$$\frac{S_c}{D_i} = Fr^{0.154} Re^{-0.315} We^{0.462} (\psi)^{0.071} \tag{2.14}$$

Where ψ is a parameter, equal to $[(b_1+b_2)/Di].(b_1/b_2)$. b_1 is the small side wall clearance, which is the distance between the intake pipe centerline and the closer side wall to the intake pipe, and b_2 is the large side wall clearance, which is the corresponding distance for the other wall.

CHAPTER 3

MODELLING OF AIR ENTRAINING VORTICES

3.1. Introduction

In the solution of problems related to hydraulics, many experimental and some theoretical studies have been conducted. However, experimental research has generally been preferred rather than computational or theoretical studies due to some reasons. Before construction of many hydraulic projects, which needs huge investments, small scale hydraulic models are tested in order to obtain feasible solutions. Theoretical solutions may give unrealistic results because they may ignore the unseen reasons behind the problems. Also, computational solutions may underestimate the real case situation due to complexity of the phenomenon. Because of these reasons, scale modelling of prototype is inevitable solution for many hydraulic structures before designing and construction.

Air-entrained vortex formation at free water surface is one of the major complicated problem for intake structures. The vortex formation depends on approach flow conditions, geometrical properties of the structure and fluid properties that are used in the experiments. Considering all the above-mentioned properties, experimental studies are preferred to investigate the vortex formation at intake structures.

3.2. Application of Dimensional Analysis to the Related Parameters

The parameters related to the formation of vortex study are divided in three groups;

- Flow Properties: Average velocity of flow in the intake pipe (V_i), average circulation imposed to flow (Γ) and gravity acceleration (g).
- Fluid Properties: Fluid density (ρ), dynamic viscosity of the fluid (μ) and surface tension of the fluid (σ).
- Geometric Properties of the Intake and Reservoir: Intake pipe diameter (D_i), the distance between the right and left approach channel side walls at the frontal face of the intake structure (W), the vertical distance between the bottom point of the intake and the base of the reservoir (a), and the angles between the approach channel side walls and the front face of the intake structure (θ). In this study, it is assumed that the approach channel side walls are sufficiently long and therefore their lengths are not considered as additional parameters in the analysis.

Considering the common type of a horizontal intake as shown in Figure 3.1, S_c is defined as the critical submergence, which is the distance between the free surface level and the intake at which air- entraining vortex form. So, Sc can be described as a function of the independent variables as given below;

$$S_c = f_1\ (\rho, \mu, \sigma, g, V_i, \Gamma, D_i, a, W,\ L, \theta) \tag{3.1}$$

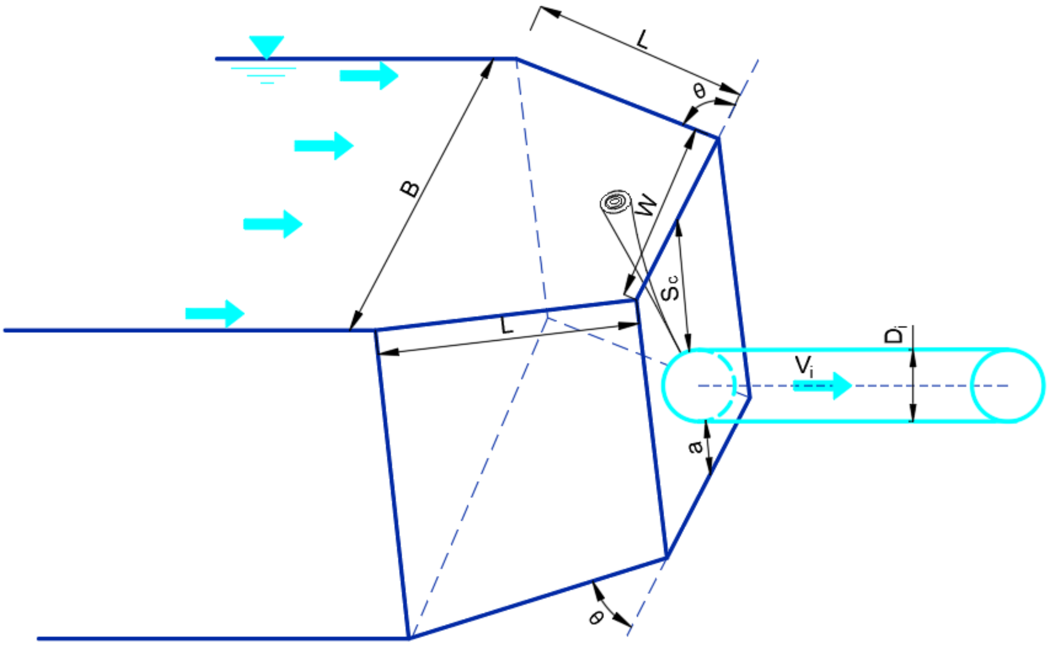

Figure 3.1 Horizontal Intake Structure Sketch with geometrical parameters

After Buckingham's π theorem applied to Equation 3.1, the dimensionless terms given below are obtained;

$$\frac{S_c}{D_i} = f_2\left(\frac{W}{D_i}, \frac{L}{D_i}, \frac{a}{D_i}, \mathrm{Fr}, \mathrm{Re}, \mathrm{We}, K_0, \theta\right) \tag{3.2}$$

where

$\frac{W}{D_i}, \frac{L}{D_i} =$ Dimensionless terms related to the geometrical parameters

$\frac{a}{D_i} =$ Ratio of bottom clearance to intake diameter

$\mathrm{Fr} =$ Intake Froude number $= \frac{V_i}{\sqrt{gD_i}}$

$\mathrm{Re} =$ Intake Reynolds number $= \frac{V_i D_i \rho}{\mu}$

$\mathrm{We} = $ Intake Weber number $= \dfrac{\rho V_i^2 D_i}{\sigma}$

$K_0 = $ Intake Kolf number $= \dfrac{\Gamma}{D_i V_i}$

$\theta = $ the angles between the side walls and the front face of the intake structure

In this study, the vertical distance between the intake pipe and bottom of the reservoir, called as bottom clearance a, is zero. Thus, $\frac{a}{D_i}$ parameter can be removed from Equation 3.2. Equation 3.2 can be expressed in the form of Equation 3.3

$$\frac{S_c}{D_i} = f_2\left(\frac{W}{D_i}, \frac{L}{D_i}, \mathrm{Fr}, \mathrm{Re}, \mathrm{We}, K_0, \theta\right) \tag{3.3}$$

Within the scope of this study the length of the approach channel was assumed to be as L=100cm for the case of θ=90° although the actual length was 200cm. For other approach channel configurations tested, θ=77° and 66°, the lengths of the approach channel became a little larger than 100cm for a given θ, resulting in numerically very close values of L/D_i. Therefore, for a selected θ case, one may eliminate the term of L/D_i from Equation 3.3.

$$\frac{S_c}{D_i} = f_2\left(\frac{W}{D_i}, \mathrm{Fr}, \mathrm{Re}, \mathrm{We}, K_0, \theta\right) \tag{3.4}$$

Equation 3.4 is valid for a prototype and its model. In order to satisfy a complete similarity between the prototype and model, all the corresponding π terms must be the same in both systems. This condition results in for the length ratio of the model as $L_r=1$ if the same fluid is used in both systems. This situation is not practically possible, therefore, some parameters that are less important for formation of vortices, should be omitted from the general equation. Since the vortex formation is a free surface phenomenon and is affected by gravity, Reynolds and Weber numbers may be neglected and Froude number is selected as a main parameter.

3.3. Effect of Froude Number

Past studies related with formation of vortices state that Froude number is the most important dimensionless parameter for the vortex formation. For example, Gordan (1970) revealed that critical submergence was only expressed as a parameter of Froude number. Therefore, Froude similitude law was used to model the air-entraining vortices, however, this results in incomplete similarity of model and prototype, which causes scale effect. Moreover, in order to ignore effect of viscous and surface tension forces on the model, many of past studies stated limit values for Reynold and Weber numbers, which are discussed in the next titles.

3.4. Effect of Reynolds Number

In hydraulics, Reynolds number is one of the important dimensionless parameters especially in pipe flows, which shows the viscous effect of flow on the phenomenon. It was stated in the past studies that effect of Reynolds number on the formation of vortices can be negligible if it exceeds a certain limit value. After Radial Reynold number, Re_R, exceeds $3x10^4$, its effect on vortex formation can be negligible. Also, Jain et al. (1978) stated that when Reynold number, Re, is greater than $2.5x10^3$, its effect on vortex formation is negligible.

3.5. Effect of Weber Number

Surface tension forces in the flow are associated with Weber number, which is a dimensionless parameter. Weber number similarity should be satisfied to avoid scale effect on dynamic similarity of model. However, when Froude similitude law is used for a small scaled model, similarity of Weber number can not be used for this model. This scale effect problem has been investigated by many researchers. Weber number can also be ignored if it exceeds a limit value as it is in Reynolds Number. Anwar (1977) stated that effect of surface tension forces is negligible when Weber number exceeds $1.2x10^2$. Similarly, Jain (1978), Padmanabhan and Hecker (1984) stated that effect of Weber number on the formation of vortices is independent from surface tension forces, if the limit values are larger than 6×10^2 and 3.2×10^3 respectively.

3.6. Effect of Kolf Number

Kolf number is a dimensionless parameter which indicates effect of circulation on the flow. Main parameters for circulation consist of approach flow conditions, geometric properties of water intake structure and discharge of the flow. All these parameters are shown in Equation 3.4. In this study, circulation parameter Γ can be removed from equation 3.4 since no forced circulation is created. Therefore, the final form of the equation is shown below for symmetrical approach flows;

$$\frac{S_c}{D_i} = f_2\left(\frac{W}{D_i}, Fr, Re, We, \theta\right) \tag{3.5}$$

CHAPTER 4

EXPERIMENTAL SETUP AND METHODOLOGY

4.1. Experimental Setup

The experimental study has been conducted in METU Hydromechanics Laboratory to observe the formation of vortices at horizontal intake structures. The experimental setup consists of a large reservoir, an approach channel with adjustable side walls, horizontal intake pipe and a rectangular open channel with a sharp-crested weir at the end to measure the flow discharge. The reservoir has a rectangular plan view with dimension of 310x310m and 220cm height as seen in Figures 4.1 and 4.2. Figures 4.3-4.5 show the photographs of the experimental setup, which are taken from different points of view. Side and rear walls of the reservoir are concrete and front face is plexiglass to enable visual observation of vortex formation. Moreover, the horizonal intake pipe, made of plexiglass, is mounted into the frontal plexiglass wall. The reservoir is fed by one steel pipe with a valve, located at the back side of the rear wall. Another steel pipe at the back side is used to drain the reservoir. The reservoir has both dead and active volumes. Dead volume is at the bottom of the rigid slab diaphragm in order to decrease the effect of turbulence on the incoming flow. The zone, above the rigid slab diaphragm, can be defined as active volume. Also, there is a screen layer, which is made of bricks, at the rear side of the active volume in order to provide uniform flow to the active volume though the horizontal intake pipe (Figure 4.6). At the beginning of the experiment, water fills the dead volume of the reservoir. After dead volume is full of water, water level begins to increase at the active volume of the reservoir. After water level reaches a specific level, vortex formation is observed for different pipe and approach flow wall-slope configurations. Water flows from the reservoir into the concrete pool by means of a plexiglass horizontal intake pipe. This pool is connected to the concrete rectangular open channel. There is a sharp crested weir at the end of the channel. This weir is calibrated with an acoustic flowmeter before conducting the experiments for each pipe to be tested. In this experimental study, three different plexiglass pipe diameters of D_i=30cm, 20cm and 10cm, as horizontal intake are used together with different approach channel wall-slope configurations. A pump is used in the model to supply adequate discharge for vortex formation when the intake pipe diameters are D_i=20cm and 10cm.

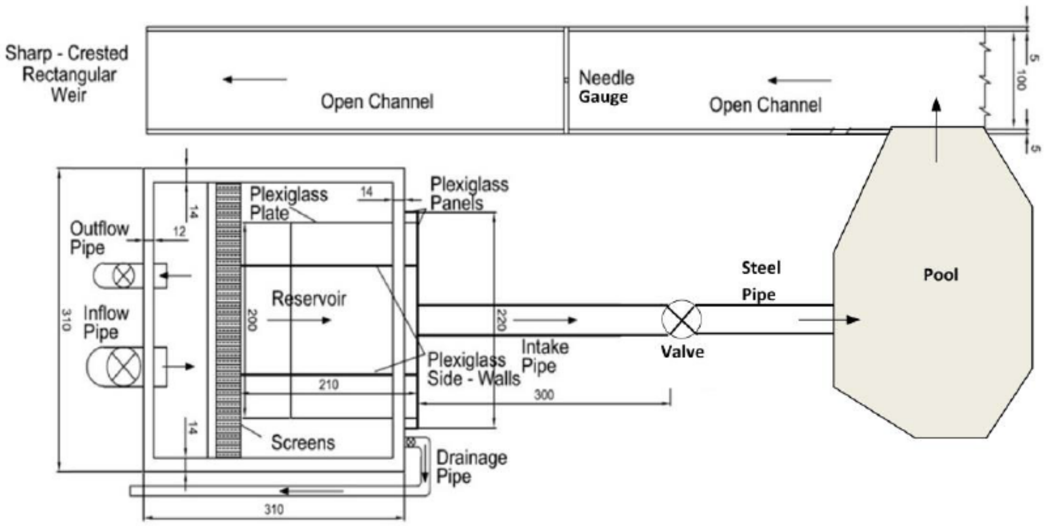

Figure 4.1 Sketch of the Experimental Setup in Plan View Without Pump (Zaloğlu, 2014)

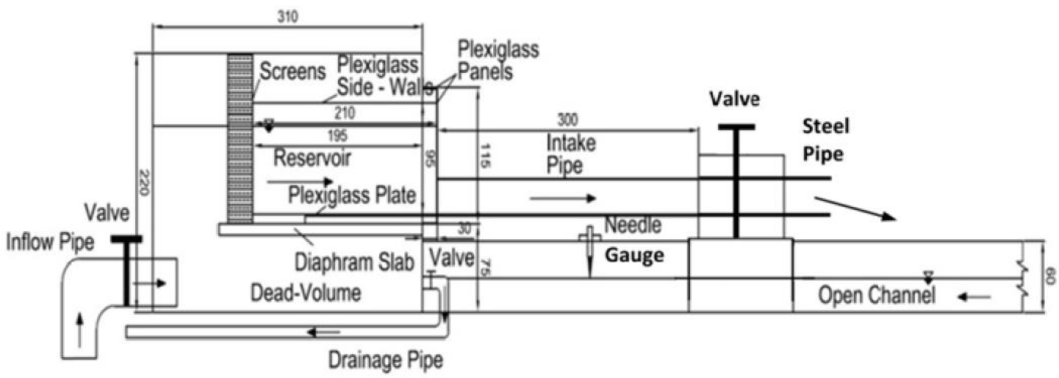

Figure 4.2 Sketch of the Experimental Setup in Side View Without Pump (Zaloğlu, 2014)

Figure 4.3 General View of the Experimental Setup

Figure 4.4 Front View of the Experimental Setup without Pump, D_i=30cm

Figure 4.5 General View of the Experimental Setup with Pump, D_i=10cm

Figure 4.6 Screen Layer and Active Volume of the Reservoir

4.2. Experimental Methodology

Approach channel side walls, made of plexiglass, were attached to the front face and existing plexiglass side walls with a certain angle by using silicon binder before starting the experiment and this process was repeated for each set of the experiment. After approach channel side walls were attached, at least one day was waited to have the silicon binder dried. After that, concrete reservoir was filled with water by opening the inflow pipe behind the concrete rear wall. Then, the valve at the horizontal pipe, was opened slowly to avoid vibration and fluctuation on the free water surface. In the case of no pump, discharge in the horizontal pipe was adjusted by the valve on the pipe. In the case of using the pump, the discharge was adjusted by the pump valve. After that, water level was decreased slowly by means of using the drain pipe, which is connected to the dead volume. This process was continued during decreasing the water level very slowly until observing the suction of air bubbles into the intake. Sometimes full air core vortices and sometimes air-entrained bubble vortices, which are called as “deceptive vortices” were observed. These types of vortices form due to disturbances in the flow pattern and unsteady nature of the flow in the reservoir. To overcome this misleading formation and ensure that the vortices were not deceptive, each test was performed at least two times for the same setup and flow conditions. After ensuring that the vortex was not deceptive, the discharge was read from acoustic flowmeter and the water level was measured from the piezometer tube (Figure 4.7). In this study, this process was repeated for three different intake pipe sizes. For each pipe, three different approach channel side-wall angles were examined. Therefore, one set of the experiment was performed for one intake pipe diameter, and one approach channel side-wall angle at various discharges. In each experimental set at least 5 different discharge values were tested. Figures 4.8-4.16 show the sketches of the plan views and photographs of the experimental setup.

Figure 4.7 Piezometer Tube and Acoustic Flowmeter Used in the Experiments

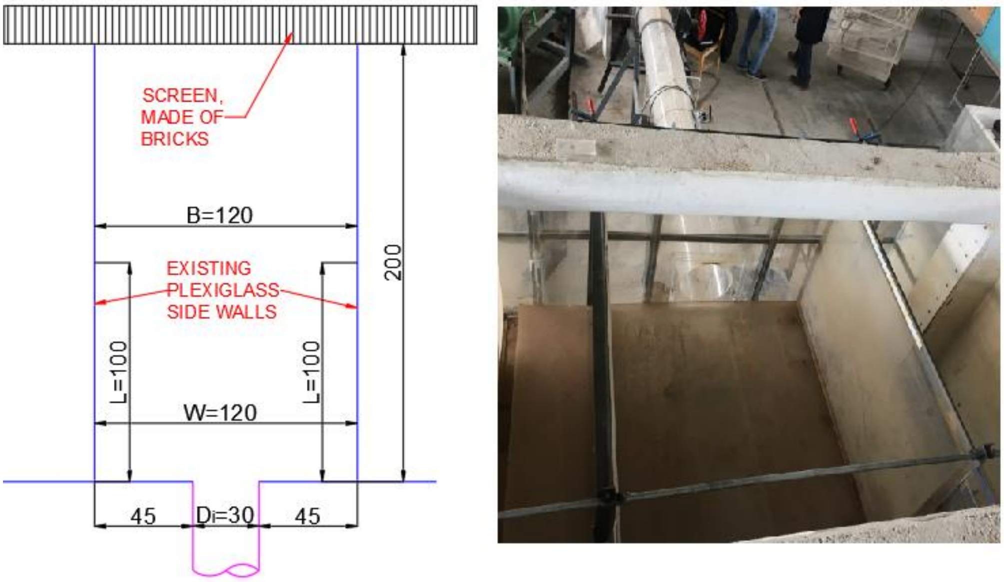

Figure 4.8 Sketch of Plan View and a Photo of the Experiential Setup for D_i=30cm, W/D_i=4.00, L/D_i=3.33 and $\theta=90^0$ (dimensions are in cm)

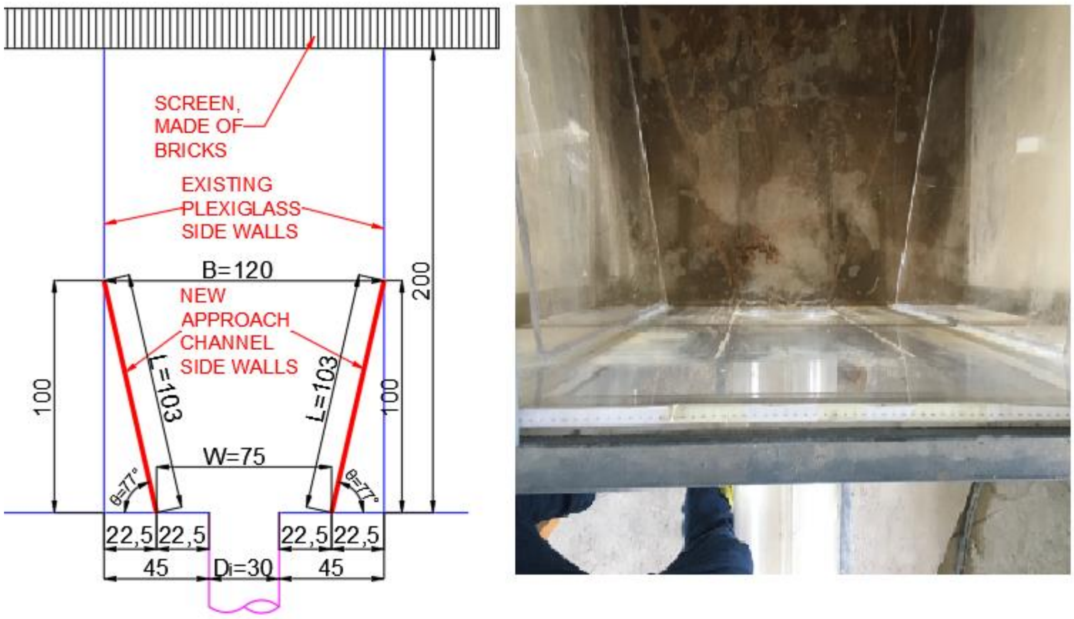

Figure 4.9 Sketch of Plan View and a Photo of the Experiential Setup for D_i=30cm, W/D_i=2.50, L/D_i=3.43 and $\theta=77^0$ (dimensions are in cm)

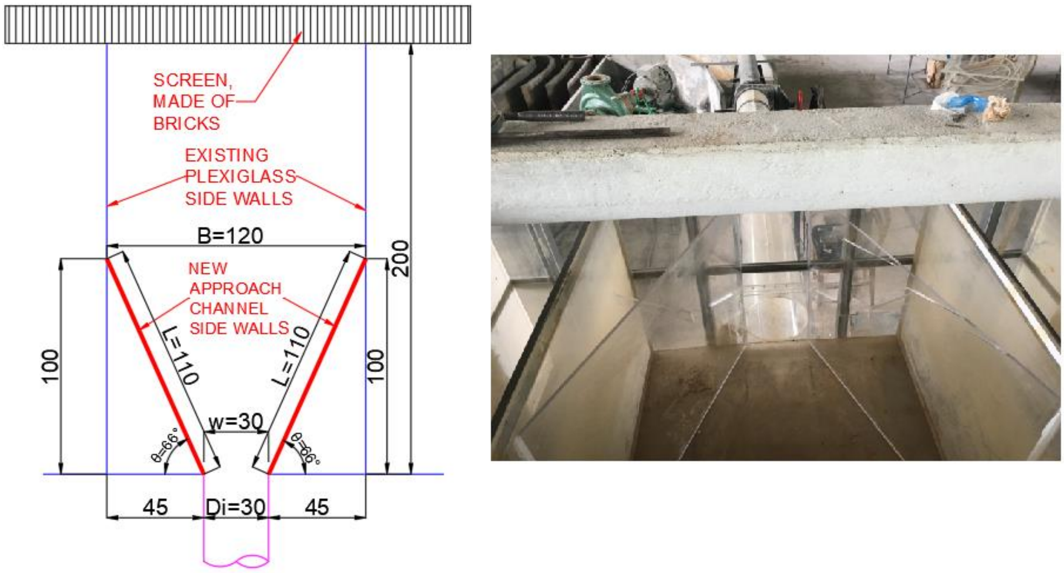

Figure 4.10 Sketch of Plan View and a Photo of the Experiential Setup for D_i=30cm, W/D_i=1.00, L/D_i=3.67 and $\theta=66^0$ (dimensions are in cm)

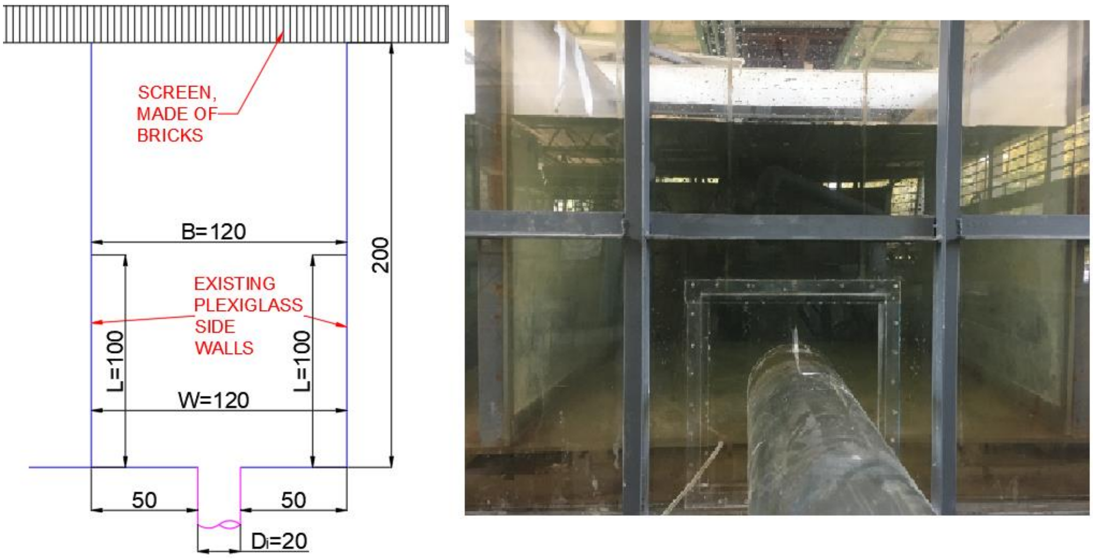

Figure 4.11 Sketch of Plan View and a Photo of the Experiential Setup for D_i=20cm, W/D_i=6.00, L/D_i=5.00 and $\theta=90^0$ (dimensions are in cm)

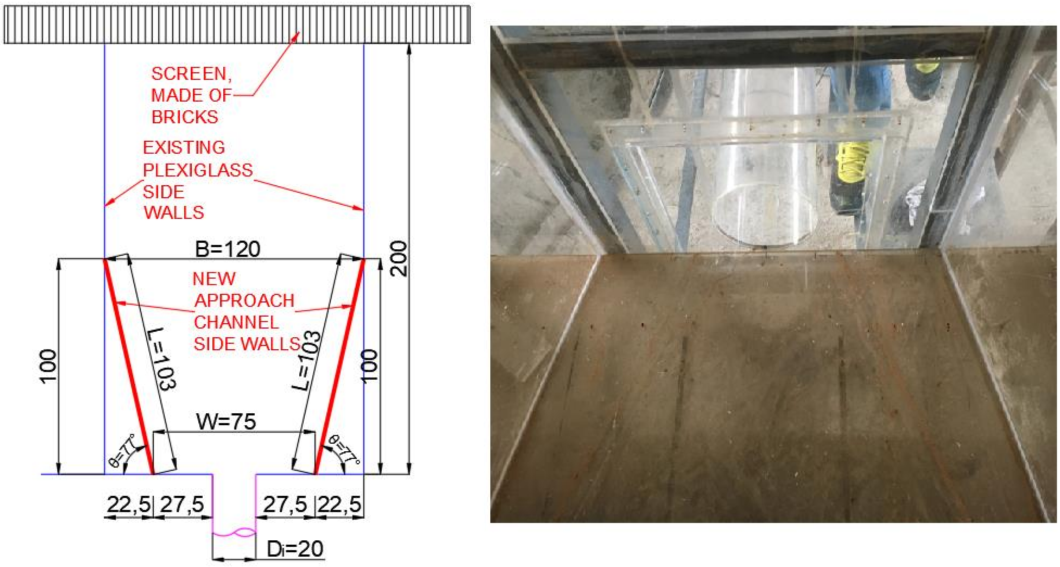

Figure 4.12 Sketch of Plan View and a Photo of the Experiential Setup for D_i=20cm, W/D_i=3.75, L/D_i=5.15 and $\theta=77^0$ (dimensions are in cm)

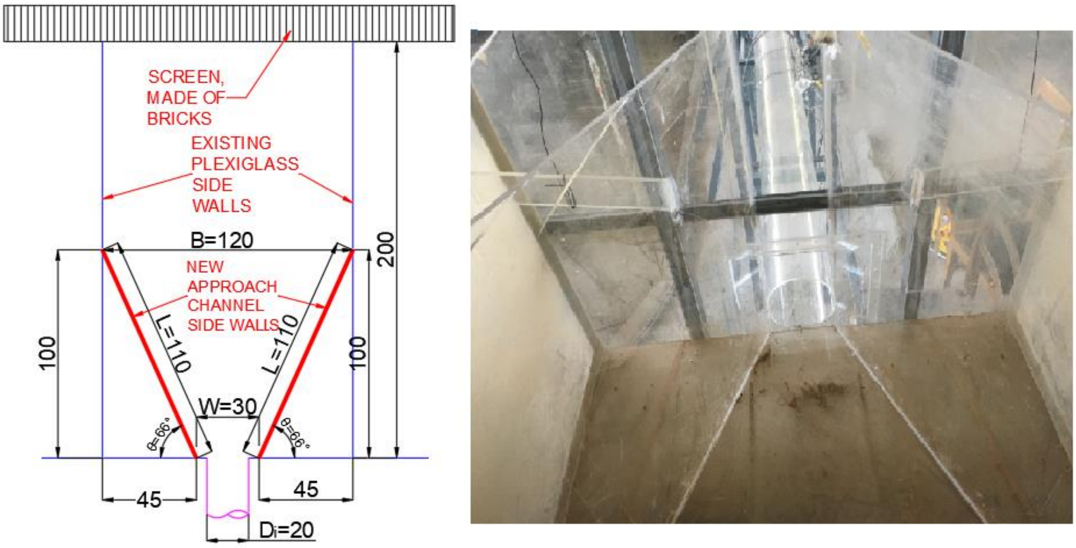

Figure 4.13 Sketch of Plan View and a Photo of the Experiential Setup for D_i=20cm, W/D_i=1.50, L/D_i=5.50 and $\theta=66^0$ (dimensions are in cm)

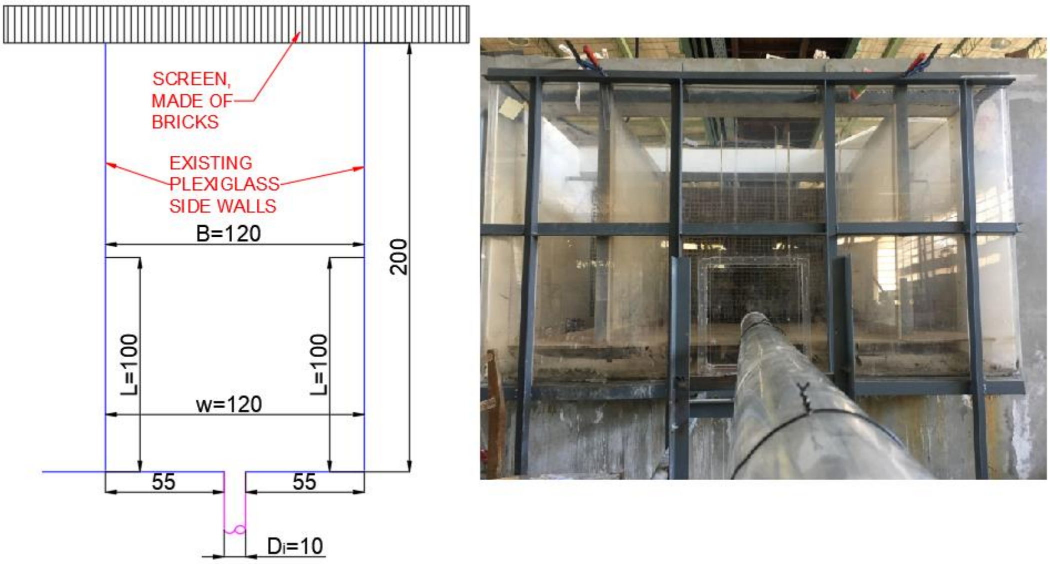

Figure 4.14 Sketch of Plan View and a Photo of the Experiential Setup for D_i=10cm, W/D_i=12.0, L/D_i=10.0 and $\theta=90^0$ (dimensions are in cm)

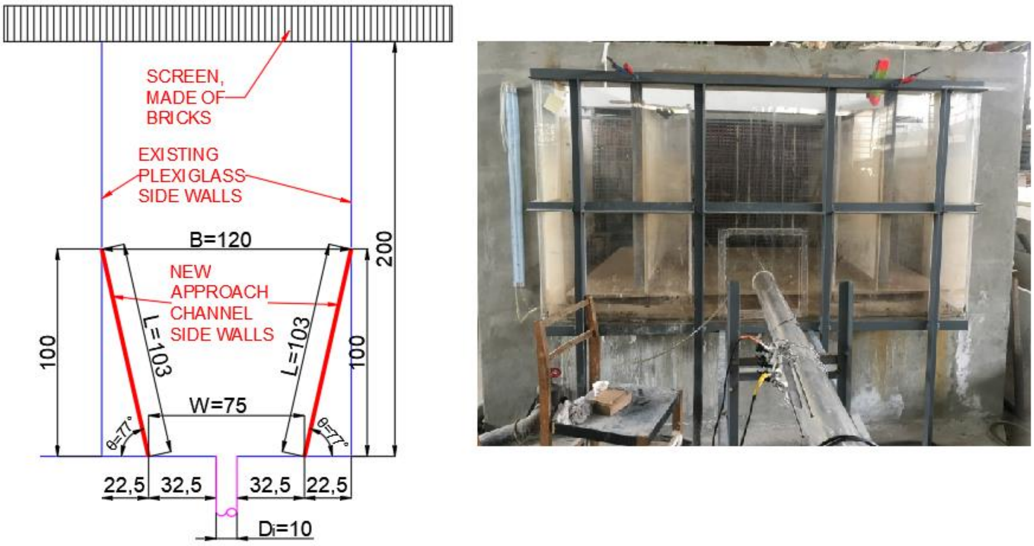

Figure 4.15 Sketch of Plan View and a Photo of the Experiential Setup for D_i=10cm, W/D_i=7.50, L/D_i=10.3 and $\theta=77^0$ (dimensions are in cm)

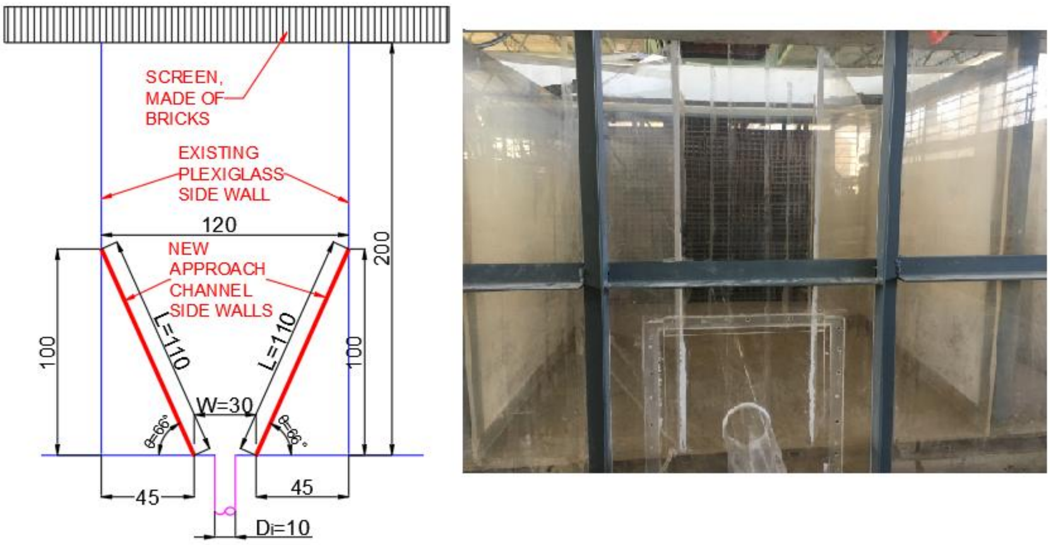

Figure 4.16 Sketch of Plan View and a Photo of the Experiential Setup for D_i=10cm, W/D_i=3.00, L/D_i=11.0 and $\theta=66^0$ (dimensions are in cm)

4.3. Vortex Observations

Many vortex formations were observed during the experiments. These vortices usually occurred in a sequence, which were defined by Alden Research Laboratory. At the beginning, eddies are observed at free water surface. These eddies turn into dimples with small decrease in water level. When water level decreasing slowly, the dimples gain strength and finally air-entrained bubbles and vortex tail are formed. Therefore, according to the observations, formation of vortices occurs in order of; surface disturbance, swirl motion, formation of eddies, dimples, vortex pulling floating trash, vortex pulling air bubbles and finally full air core. In this study, only type 6 vortices were taken into consideration to determine critical submergence. Figures 4.17 – 4.19 show some photographs of the observed vortices in the experiments.

Figure 4.17 Dimple Formation on the Water Surface

Figure 4.18 Vortex Pulling Air Bubbles into the Intake

Figure 4.19 Full Air Core Vortex

CHAPTER 5

ANALYSIS AND EVALUATION OF THE EXPERIMENTAL RESULTS

5.1. Introduction

In this chapter, experimental results and its discussion are presented for symmetrical various approach flow conditions. Variation of critical submergence to intake diameter ratio, S_c/D_i, depends on Froude, Reynold and Weber numbers, W/D_i and θ. Necessary geometric and hydraulic data such as distance between the right and left approach channel side walls, discharge, velocity and critical submergence were noted during the experiments to calculate the relevant dimensionless parameters, which are indicated in Equation 3.5 and tabulated in the Appendix. Then, graphical representations were used for the analysis of the data obtained from experiments. Regression analysis was applied to the data to obtain empirical equations for variation of S_c/D_i as a function of aforementioned dimensionless parameters.

Three different intake pipe diameters were tested and effects of various approach channel shapes on critical submergence were discussed. Table 5.1 shows the ranges related with important hydraulic and geometric parameters used in the calculations for different symmetrical approach channel shapes tested.

Table 5.1 *Ranges Related with Important Hydraulic and Geometric Parameters Used in the Calculations for Different Symmetrical Approach Channel Shapes*

D_i (cm)	Interval of							Number of Obs.
	Qi (lt/s)	Sc/Di	Fr	Re	We	W/Di	θ(degree)	
30	61.002 ~ 26.983	1.203 ~ 0.217	0.503 ~ 0.223	257869 ~ 114063	3063 ~ 599	4.00 ~ 1.00	90 ~ 66	19
20	53.382 ~ 25.998	1.550 ~ 0.745	1.213 ~ 0.591	338486 ~ 164846	7919 ~ 1878	6.00 ~ 1.50	90 ~ 66	15
10	42.897 ~ 20.359	3.510 ~ 2.617	5.514 ~ 2.617	544006 ~ 258186	40895 ~ 9212	12.00 ~ 3.00	90 ~ 66	15

5.2. Flow Zones in front of the Intake Structure

Figure 5.1 (a) shows the 3-dimensional frontal view of Figure 4.8 where the bottom clearance of the intake structure a=0, the angle of the approach channel side walls $\theta=90^o$, W=B=120cm and D_i=30cm. The flow coming from the approach channel of width B=120cm is forced to pass through the entrance section of the intake structure of which the diameter is D=30cm. During this process three dead zones where rotations occur, form around the entrance section of the intake structure which are designated by zones (1), (2) and (3) as depicted in Figure 5.1. In the zones (1) and (2) which are located between the entrance section of the intake structure and the side walls of the approach flow channel, flow rotations are observed mainly over the horizontal planes. As for zone (3) which is the region just above the intake structure and extends to the free surface along the head wall of the intake structure, rotating flows occur mainly over the vertical planes. Combination of all these rotating flows increases the possibility of having strong vortices in front of the intake structure.

When the angle of the approach channel side walls decreases, such as $\theta=77^o$, the volumes occupied by zones (1), (2) and (3) decreases as seen in Figure 5.1 (b). However, the flow moving towards the intake structure through the approach channel accelerates and therefore, the intensity of the flow rotations expected in zones (1), (2) and (3) increases. As the distance between the side walls is decreased, the flow velocity in the approach channel and therefore, frictional drag of the side walls on the flow will increase and finally, the horizontal area in the approach channel over which the rotational flow occurs will be a larger percentage of the total area (Gogus et al., 2016). In this case one may expect the formation of air-entraining vortices at larger values of S_c/D_i than those of $\theta=90^o$ case of the approach channel side walls.

As $\theta=66^o$, the side walls of the approach channel coincide with the sides of the intake structure-entrance section; the dead zones of (1) and (2) are not available anymore, but there is still dead zone (1) with pretty much reduced volume (Figure 5.1 (c)). In this case the incoming flow hits the head wall of the system in zone (3) with a high velocity and then tries to move down towards the intake structure. During this process very strong disturbances occur above the intake structure due to the flow rotation in zone (3) and high-speed flow coming to the intake structure along the approach channel side walls. These flow irregularities may result in early formation of air-entraining vortices compared to the cases of $\theta=77^o$ and 90^o.

The locations and functions of the dead zones (1), (2) and (3) for the experimental setups of Di=20cm and 10cm are very similar to those explained above for Di=30cm (Figures 5.2 and 5.3).

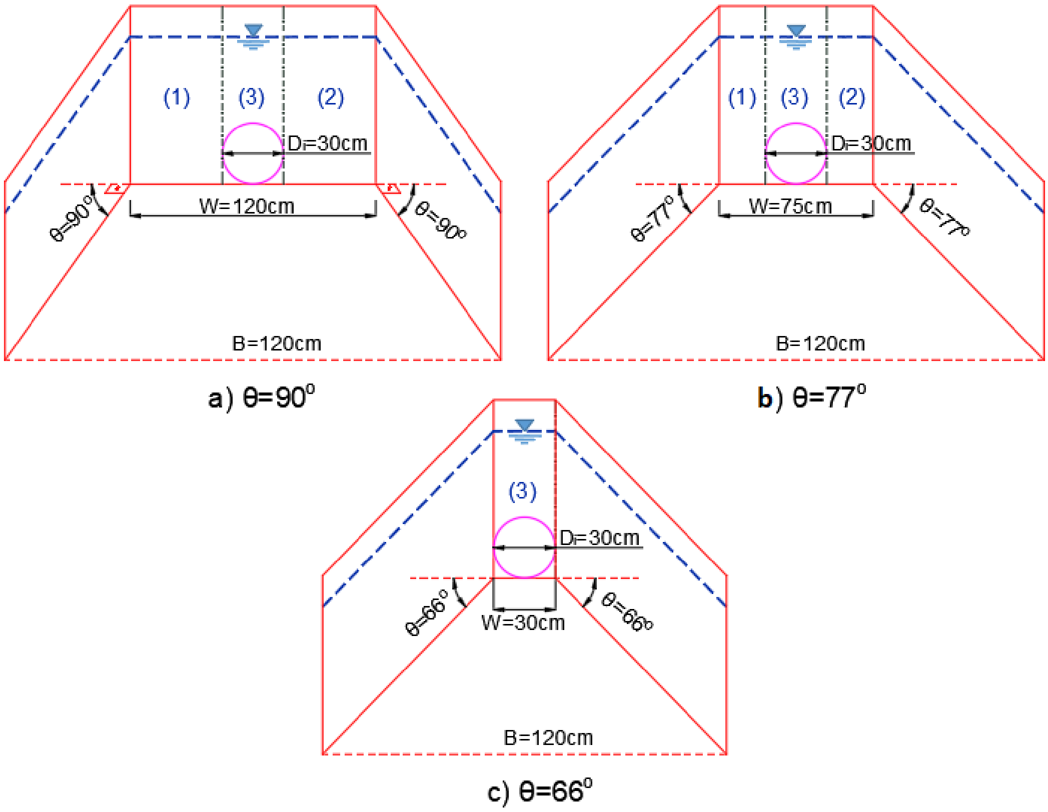

Figure 5.1 Dimensional frontal views of the experimental setups with dead zones of (1), (2) and (3) for Di=30cm; (a) θ =90º, (b) θ =77º and (c) θ =66º

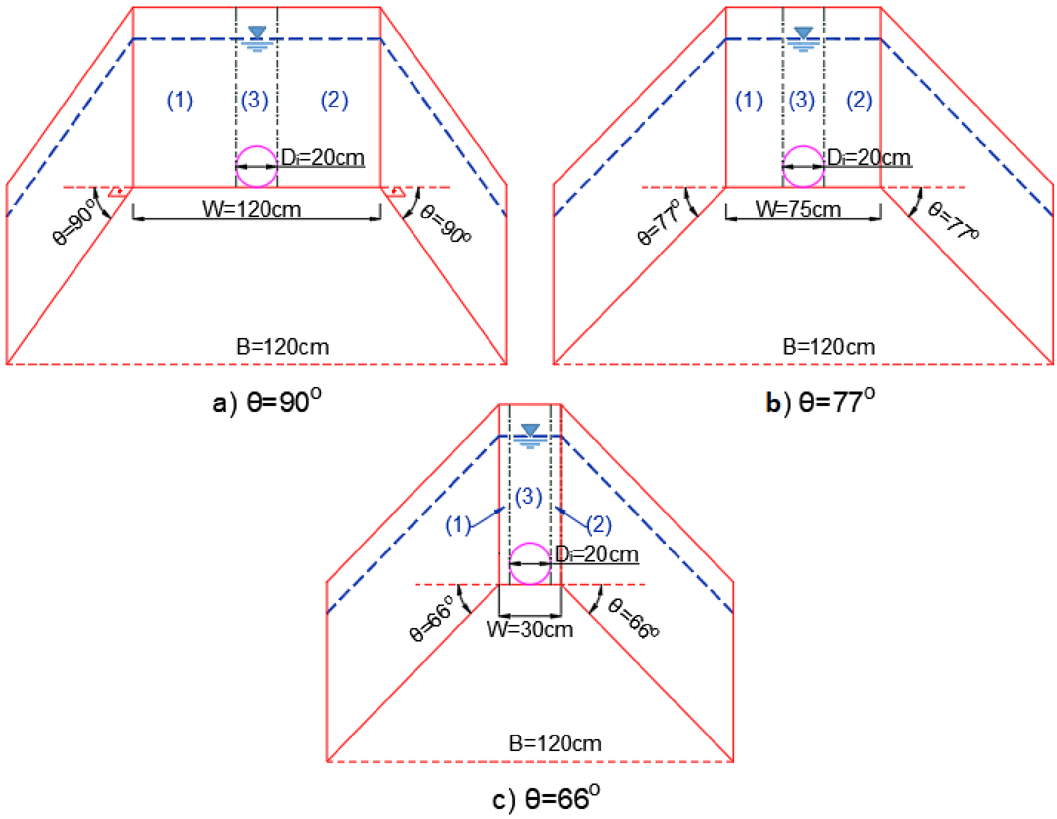

Figure 5.2 Dimensional frontal views of the experimental setups with dead zones of (1), (2) and (3) for Di=20cm; (a) θ =90º, (b) θ =77º and (c) θ =66º

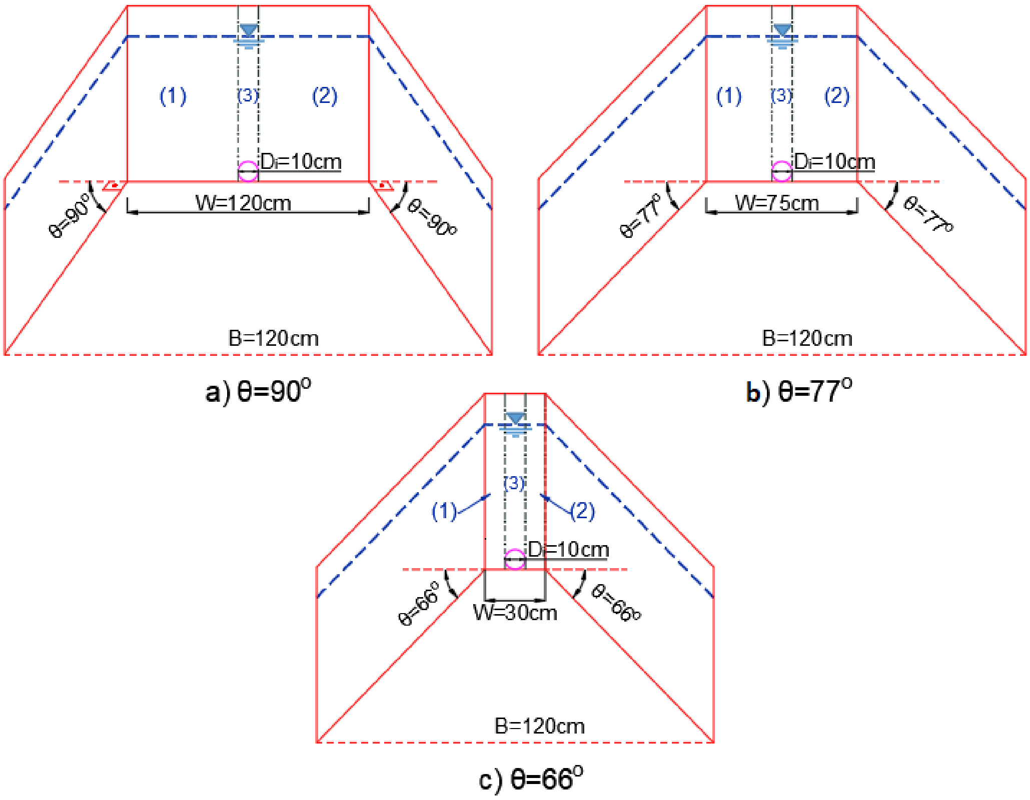

Figure 5.3 Dimensional frontal views of the experimental setups with dead zones of (1), (2) and (3) for Di=10cm; (a) θ =90°, (b) θ =77° and (c) θ =66°

5.3. Variation of S_c/D_i with Dimensionless Flow Parameters under Different Approach Flow Conditions

After necessary geometric and hydraulic data are collected from experiments, variation of S_c/D_i with Froude, Reynolds and Weber numbers as a function of W/D_i and θ were analyzed. Consequently, graphs of these parameters were presented in Figures 5.4-5.12.

In general, when all of these figures are analyzed it is seen that the trends of the measured data for S_c/D_i are very similar with Fr, Re and We for a given pipe diameter; the only difference is at the numerical values of Fr, Re and We. For a given W/D_i and θ, S_c/D_i increases with increasing Fr, Re and We. The increasing rate of S_c/D_i varies as a function of Fr, Re and We. For the pipe of D_i=30cm, up to a Froude number of about 0.35 the case W/D_i=1.00 and θ =66° gives the minimum S_c/D_i values compared to those of $\theta=77^o$ and $\theta=90^o$. For a Fr up to 0.35, the value of S_c/D_i increases with increasing θ. On the other hand, for Froude numbers larger than about 0.35, S_c/D_i values increase with decreasing θ. The reason of this situation is as explained in Section 5.2; increasing Fr means that the discharge of the system is increasing, and the rate of change of velocity of the flow through the approach channel is increasing more as the flow approaches to the intake. Therefore, maximum S_c/D_i values ae obtained for the case of minimum θ, 66^o, tested at large Froude numbers. In Figure 5.4, the observed minimum and maximum S_c/D_i values are 0.20 and 1.20, respectively, for θ values tested and Froude numbers varying between 0.22 and 0.50. From this figure it can be recommended that the approach channel side walls of $\theta=77^o$ gives the maximum S_c/D_i values for the range of Fr tested.

The results of the experiments conducted in pipes of diameters less than 30cm; 20cm and 10cm, show a little bit difference from the pipe of D_i=30cm (Figures 5.7-5.12). These figures point out that within the limits of Fr tested, S_c/D_i increases at a certain rate with increasing Fr, Re and We for a given W/D_i and θ. Minimum S_c/D_i values are obtained from the setups of D_i=20cm and 10cm for the case of $\theta=90^o$ while the maximum S_c/D_i values belong to the case of $\theta=66^o$. Since the pipe diameters are smaller than D_i=30cm in these last cases, the air-entraining vortices are obtained at larger Fr than those of D_i=30cm. Large Froude numbers imply large rates of velocities through the approach channel and therefore more intensely rotational flows in front of the intake, which result in large S_c/D_i values. For a given pipe diameter, D_i=20cm or 10cm, and Fr, the value of S_c/D_i increases with decreasing θ. The minimum S_c/D_i values are obtained with approach channel side walls angle of $\theta=90^o$ for the cases of Fr larger than 0.50. For Froude numbers larger than about 2.50, the difference between S_c/D_i values to be obtained from the setups of different θ values gets much smaller (Figure 5.10).

The related figures of S_c/D_i versus Re and We also reveal that within the ranges of Re and We tested, one can not state that S_c/D_i is independent of Re and We. Only in the figures of D_i=10cm, Figure 5.11 and 5.12, it is seen that at large values of Re and We the rate of change of S_c/D_i with the related parameters is not so important. From this point one may say that at larger values of Re and We which were not tested, the effect of Re and We on S_c/D_i may be considered negligible.

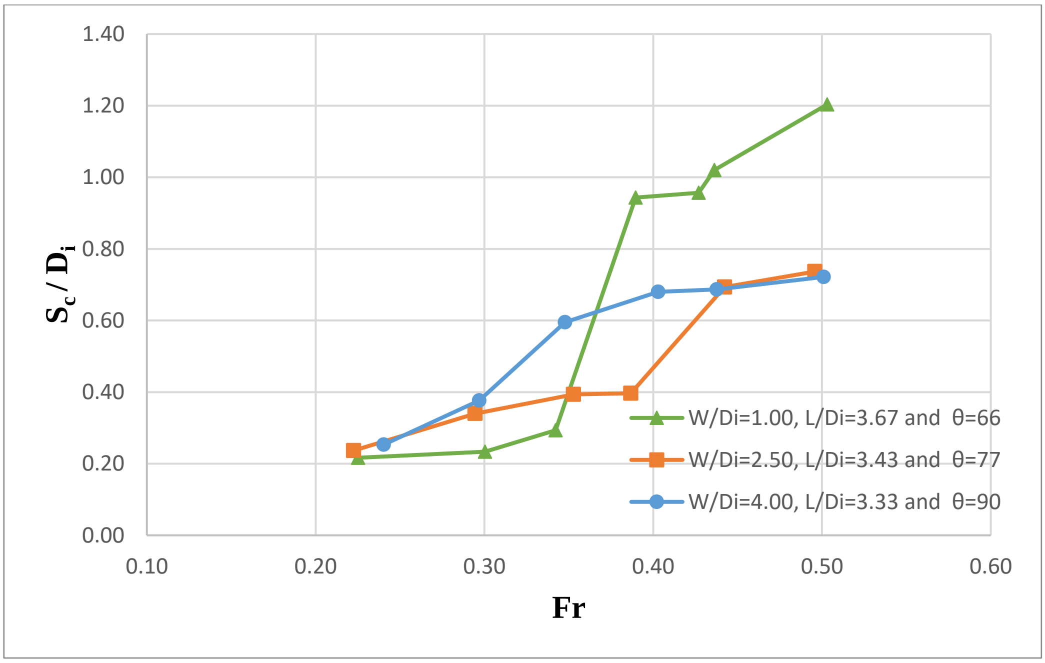

Figure 5.4 Sc/Di versus Fr for Di= 30cm as a Function of Different W/D_i, L/D_i Values and θ(degree)

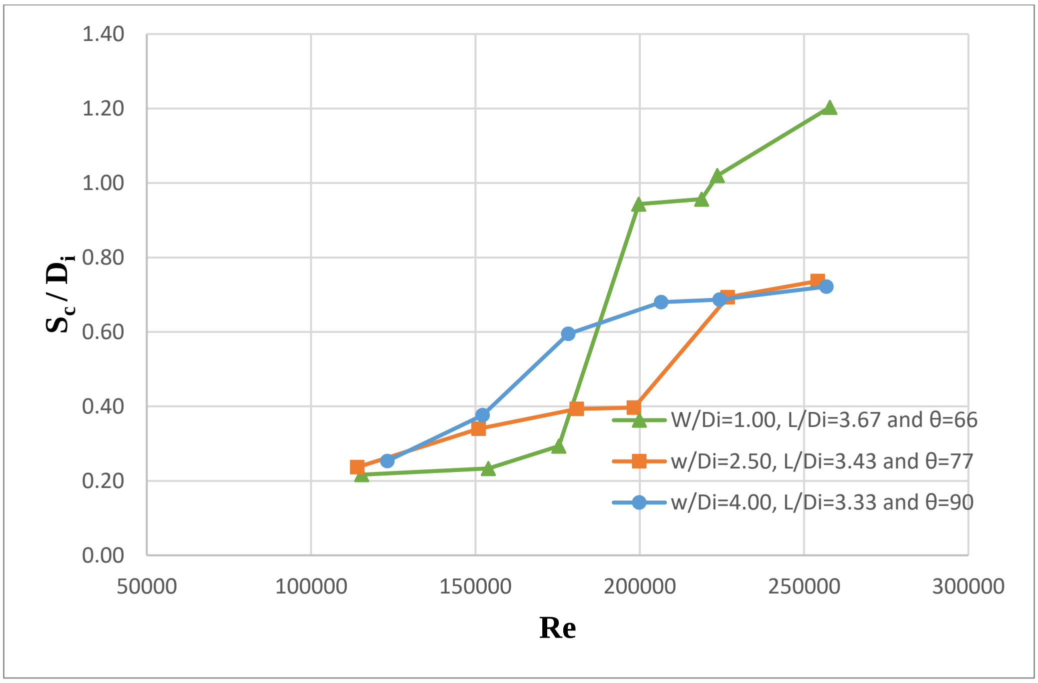

Figure 5.5 Sc/Di versus Re for Di= 30cm as a Function of Different W/D_i, L/D_i Values and θ(degree)

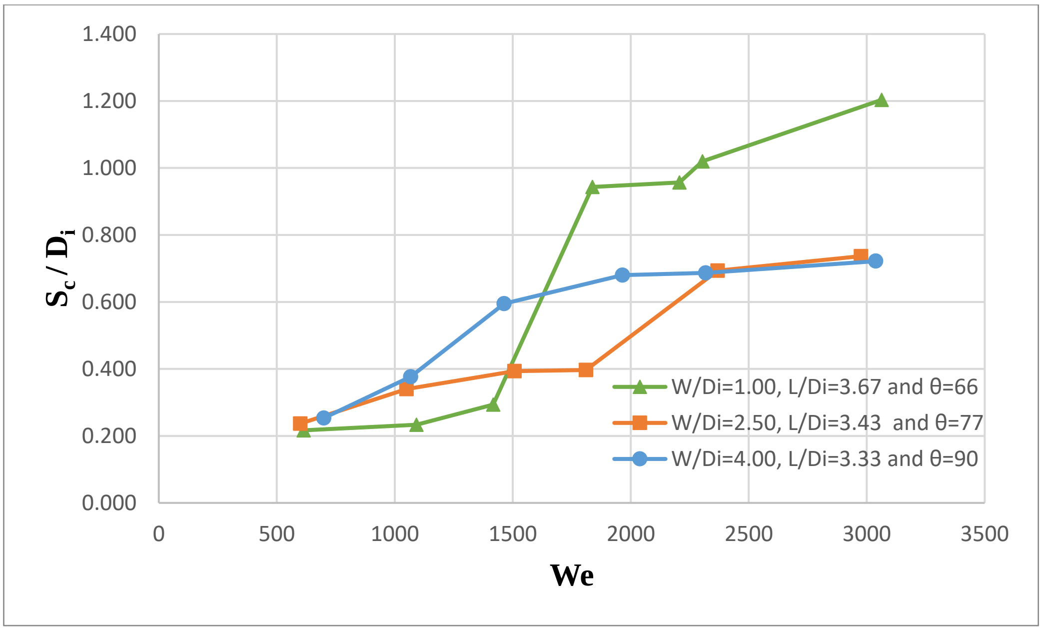

Figure 5.6 Sc/Di versus We for Di= 30cm as a Function of Different W/D_i, L/D_i Values and θ(degree)

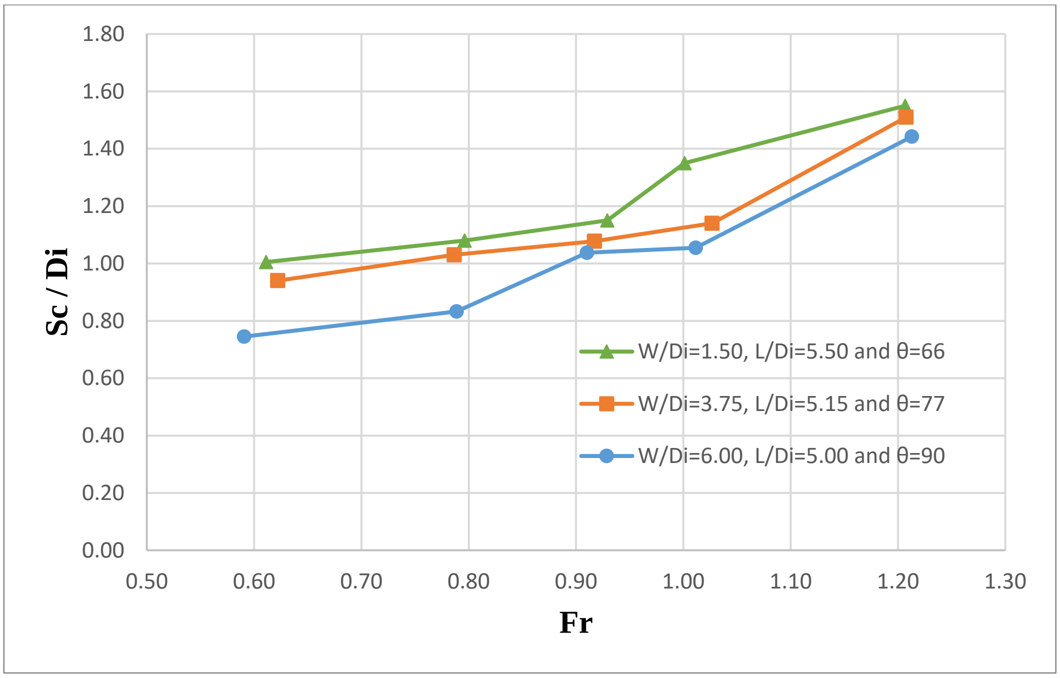

Figure 5.7 Sc/Di versus Fr for Di= 20cm as a Function of Different W/D_i, L/D_i Values and θ(degree)

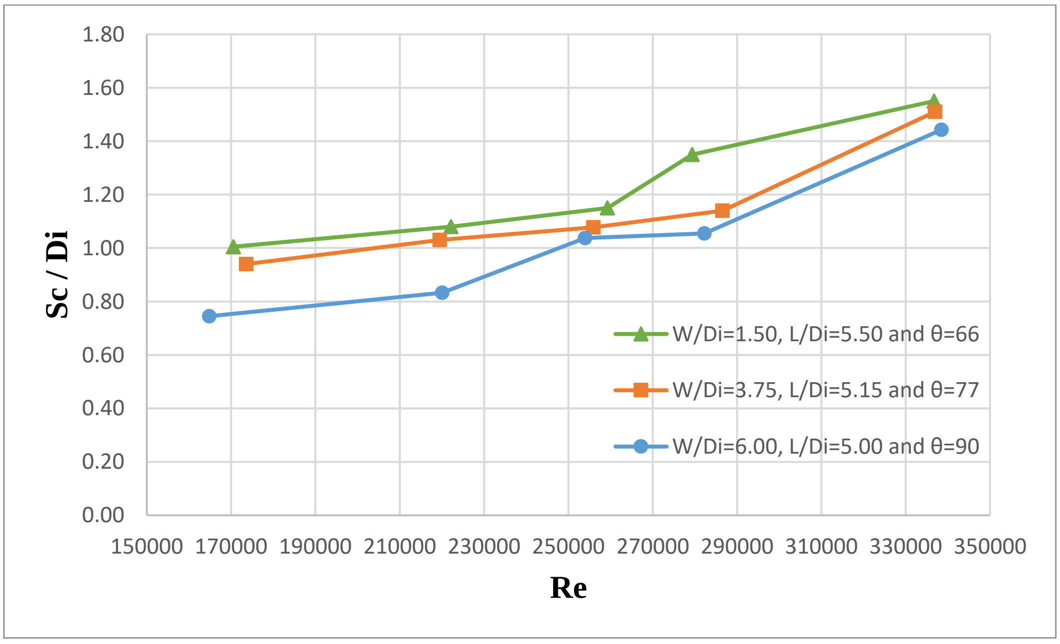

Figure 5.8 Sc/Di versus Re for Di= 20cm as a Function of Different W/D_i, L/D_i Values and θ(degree)

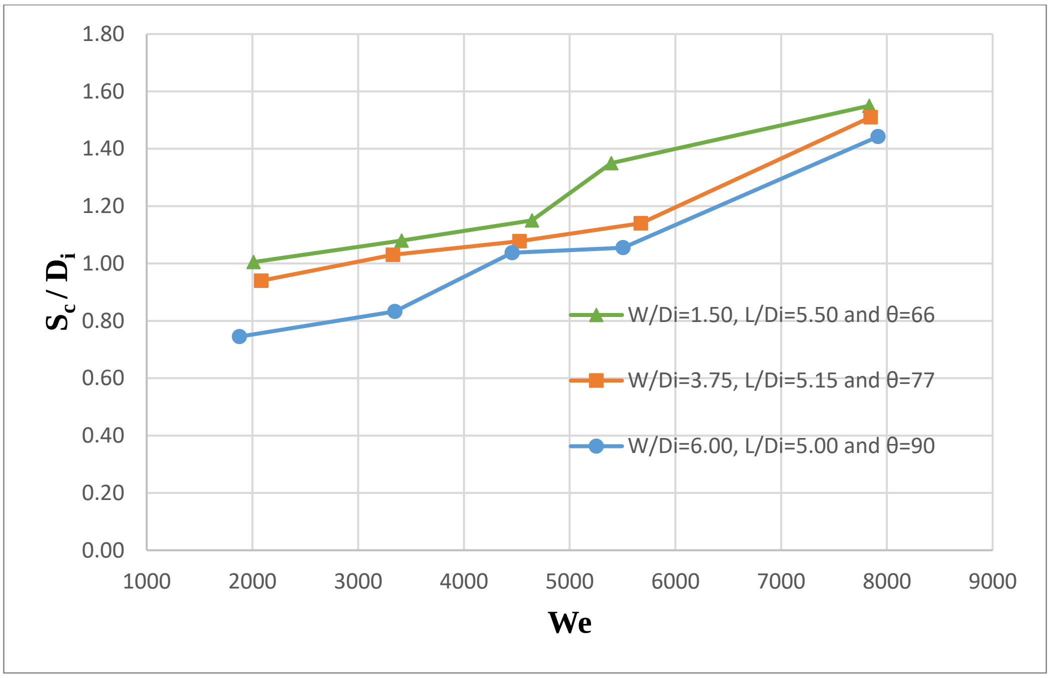

Figure 5.9 Sc/Di versus We for Di= 20cm as a Function of Different W/D_i, L/D_i Values and θ(degree)

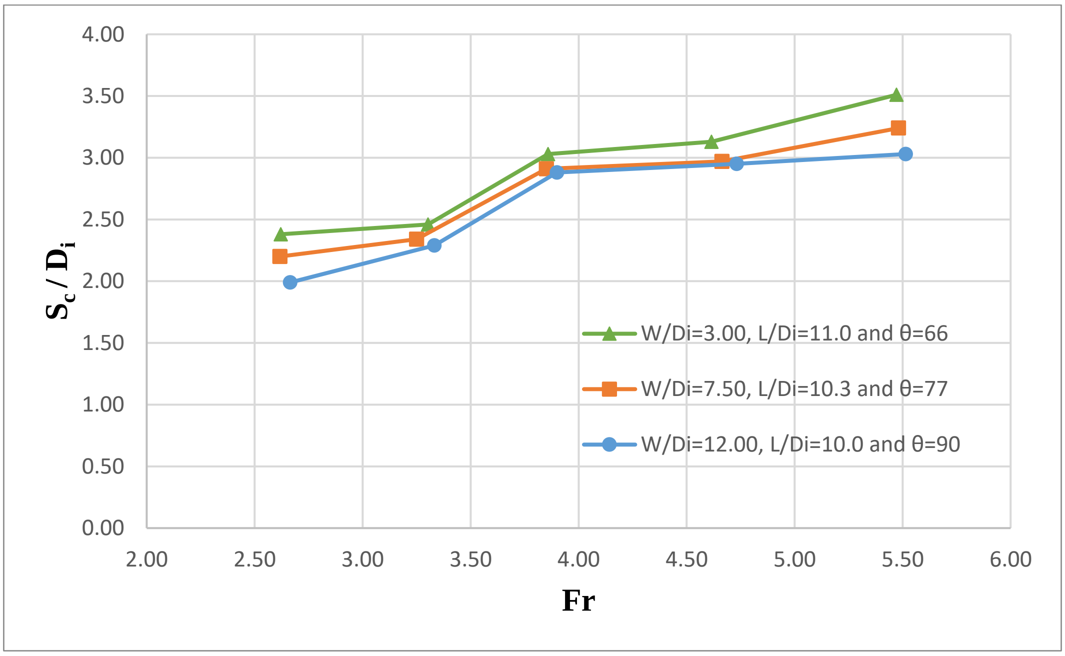

Figure 5.10 Sc/Di versus Fr for Di= 10cm as a Function of Different W/D_i, L/D_i Values and θ(degree)

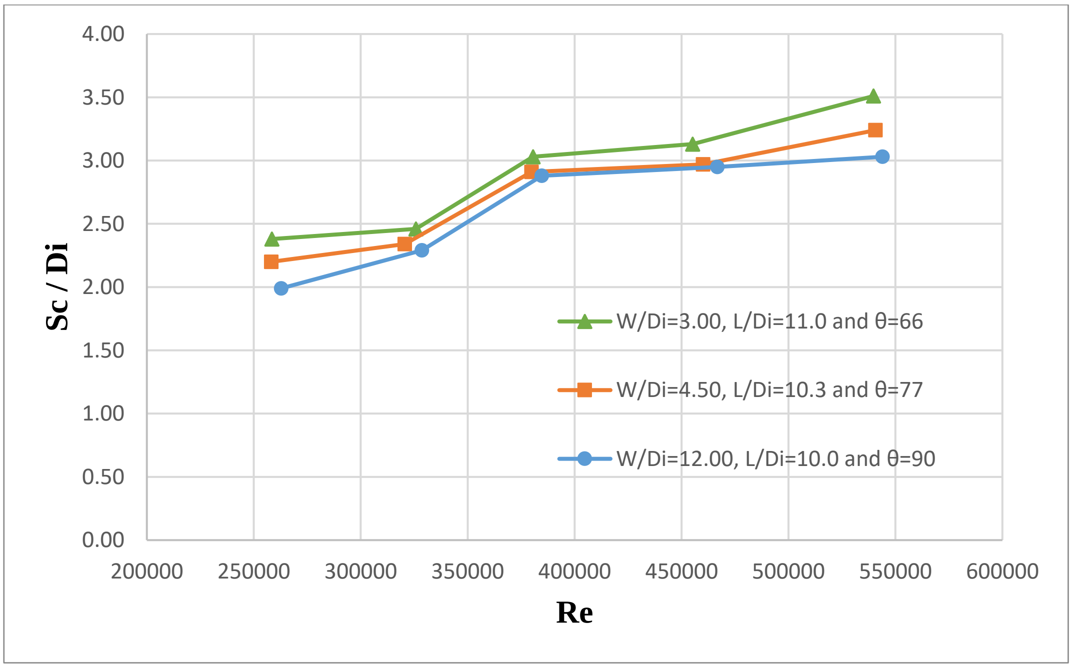

*Figure 5.11 Sc/*Di versus Re for Di= 10cm as a Function of Different W/D_i, L/D_i Values and θ(degree)

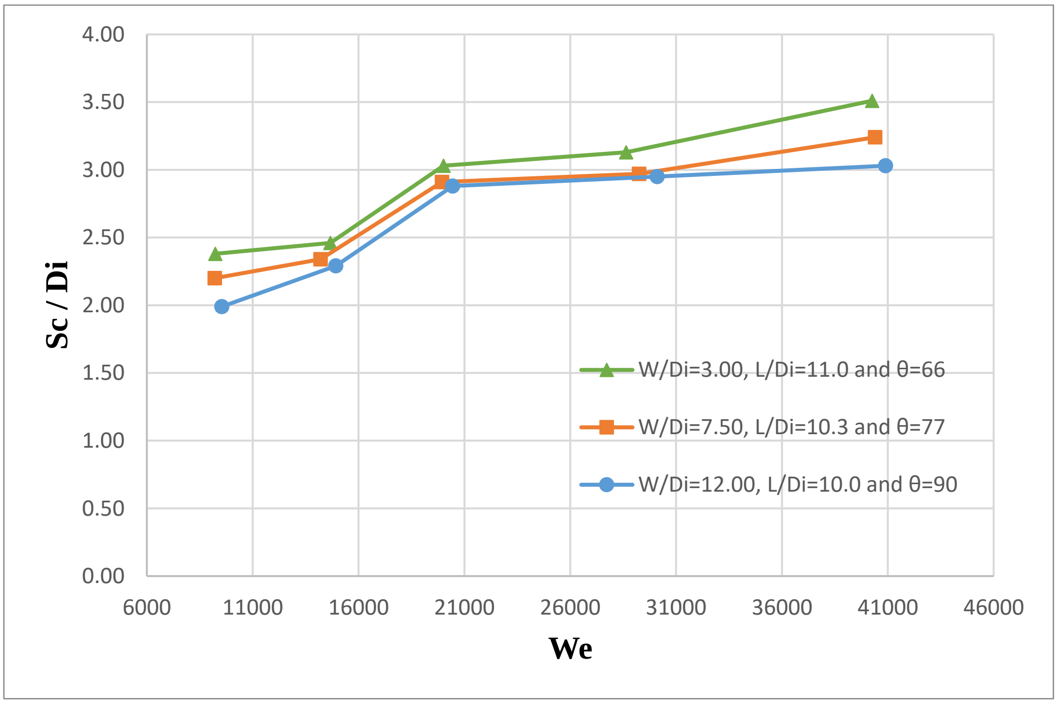

Figure 5.12 Sc/Di versus We for Di=10cm as a Function of Different W/D_i, L/D_i Values and θ(degree)

5.4. Variation of S_c/D_i with Dimensionless Parameter of W/D_i

Figure 5.13 shows the combined graph of the data points given in Figure 5.4, 5.7 and 5.10 in the form of S_c/D_i versus Fr which covers all the data obtained within the scope of this study. In general, three sets of data trends are observed in this figure. Except the data points of Fr less than about 0.35, for the remaining part of the data points lying on top of the figure belong to the experimental setup of $\theta=66^o$. The second one just below it is for $\theta=77^o$ and the last one at the bottom is for $\theta=90^o$. In this figure there is no data for the range of Fr between about 1.21 and 2.62. The reason of this is not to have related data to be obtained from the experiments of intake structures having the diameters between 10cm and 20cm.

Referring to Figure 5.13 one can plot Figures 5.14-5.16 which show the variation of S_c/D_i with W/D_i for selected constant Froude numbers. From these figures it is seen that, except the lowest Froude numbers (0.25, 0.30 and 0.40) obtained from the experiments of D_i=30cm, as W/D_i increases for a given Froude number, S_c/D_i values slightly decrease. This situation also implies that the angles of the side walls, θ, increases from 66^o up to 90^o. Figures 5.14-5.16 can be used to estimate the value of S_c/D_i for a given Fr and W/D_i.

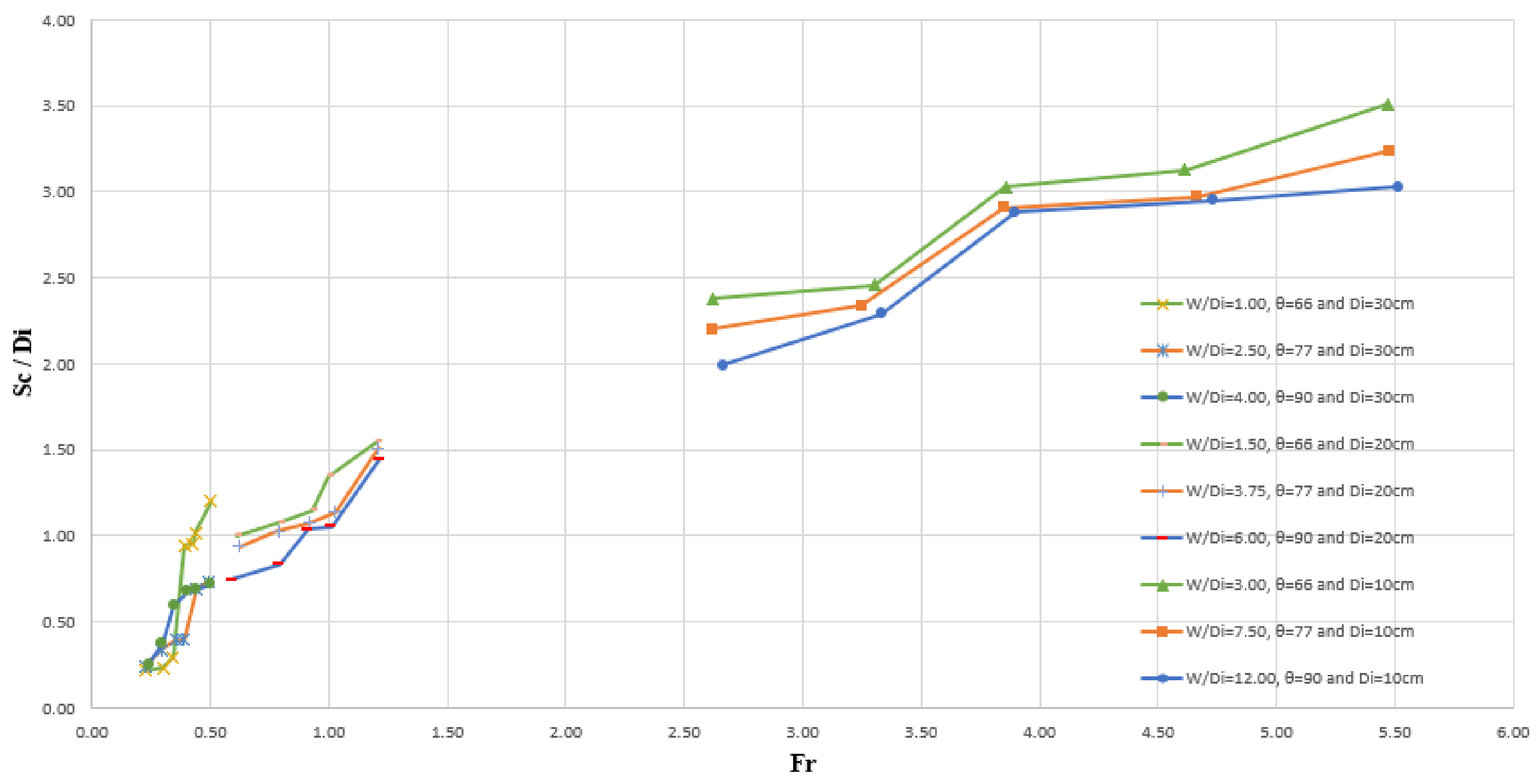

Figure 5.13 S_c/D_i Versus Fr for D_i= 10cm, 20cm and 30cm As a Function of Different W/D_i Values and θ(degree)

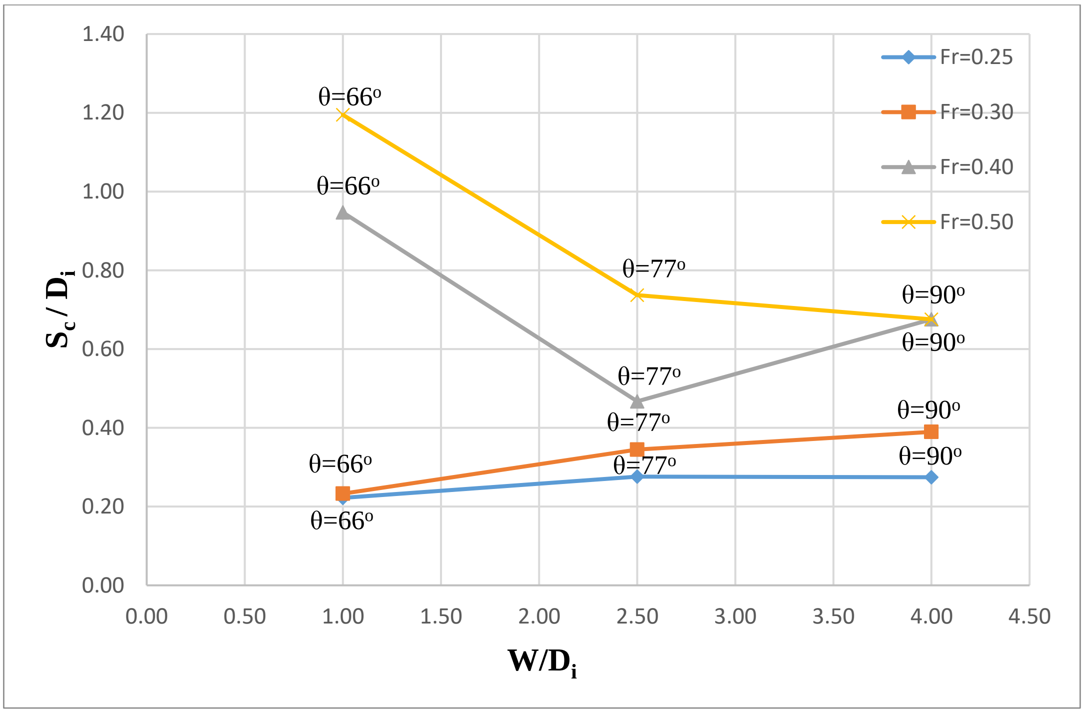

Figure 5.14 Variation of S_c/D_i *with* W/D_i *for Di= 30cm As a Function of Froude Number, Fr,*

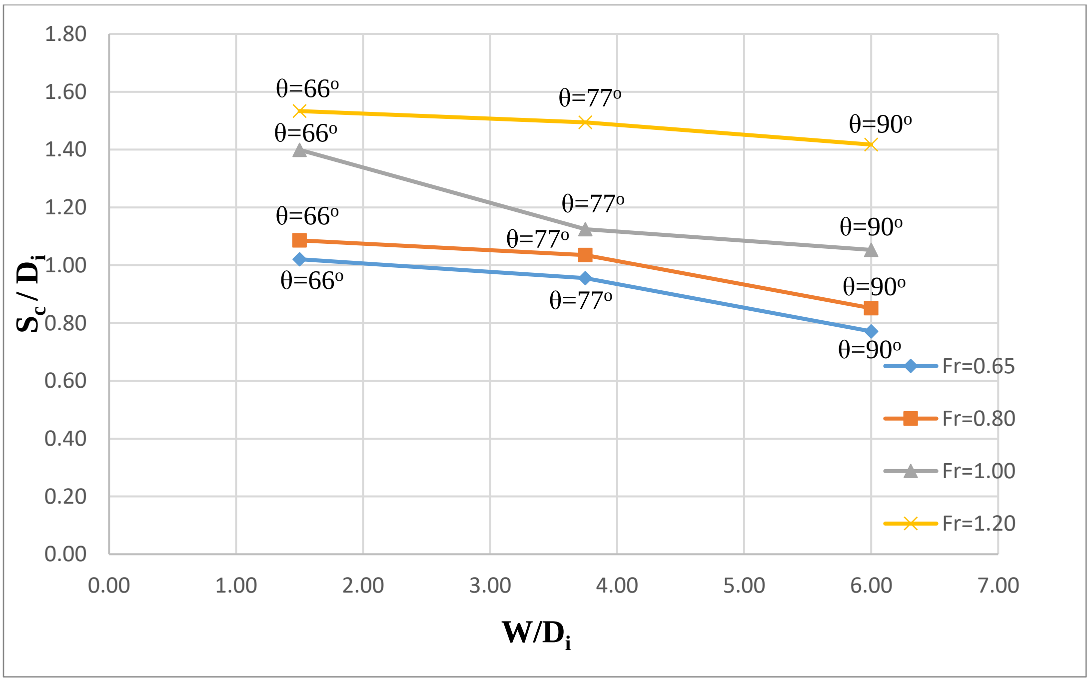

Figure 5.15 Variation of S_c/D_i with W/D_i for Di= 20cm As a Function of Froude Number, Fr,

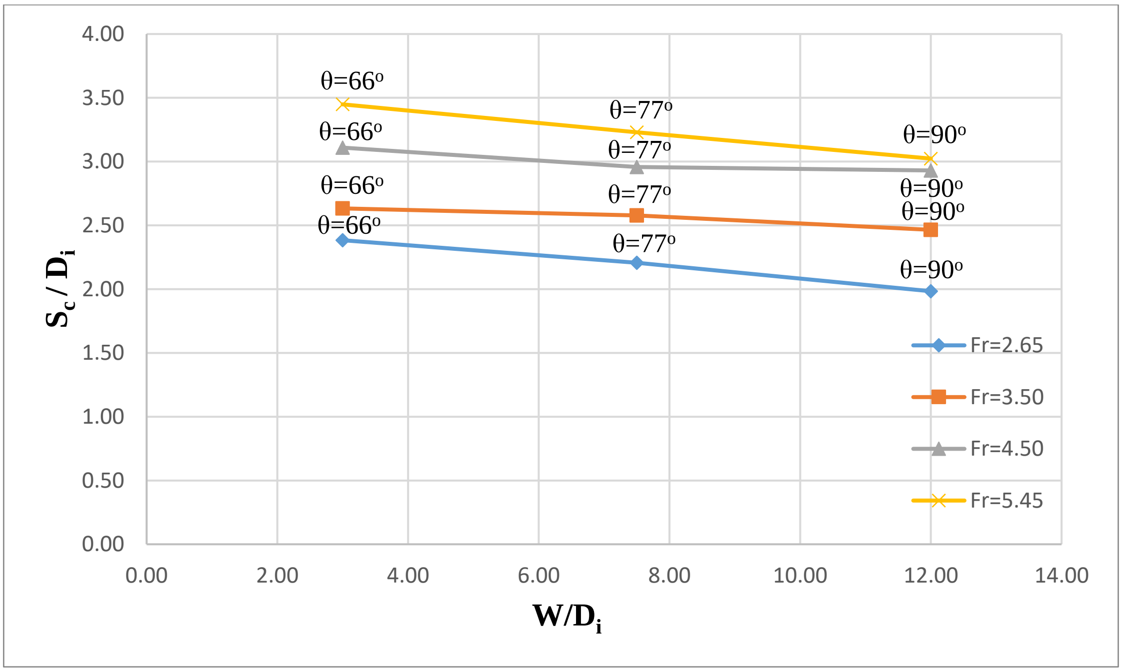

Figure 5.16 Variation of S_c/D_i with W/D_i for Di= 10cm As a Function of Froude Number, Fr.

5.5. Derivation of Empirical Formulas for Dimensionless Critical Submergence

5.5.1. The General Case

Variation of S_c/D_i depends on the dimensionless parameters indicated in Equation 3.5. By referring this equation, Equation 5.1 can be written for the dimensionless critical submergence.

$$\frac{S_c}{D_i} = \left(\frac{W}{D_i}\right)^{c1} Fr^{c2} Re^{c3} We^{c4} \theta^{c5} \tag{5.1}$$

In order to get an empirical equation of S_c/D_i, regression analysis was performed by using computer program of DataFit V9 and consequently, regression variables of c1, c2, c3, c4 and c5 were found as follows;

c1= -0.081

c2= 0.718

$c3= 0.075$

$c4= -0.078$

$c5= -0.038$

with correlation coefficient of $R^2=0.971$

After substituting the constant regression variables in Equation 5.1, the empirical equation of S_c/D_i can be given in the form of Equation 5.2. This equation is valid for the limit values of the dimensionless parameters, expressed in the Table 5.1.

$$\frac{S_c}{D_i} = \left(\frac{W}{D_i}\right)^{-0.081} Fr^{0.718} Re^{0.075} We^{-0.078} \theta^{-0.038} \tag{5.2}$$

Figure 5.17 shows comparison of the measured S_c/D_i data from experimental results and calculated S_c/D_i data from Equation 5.2. Majority of these data are within ±30% error lines, which are shown in Figure 5.17 as well. From this figure, errors between the measured and calculated S_c/D_i values were determined for each data. Consequently, variation of “percentage of data” with “values of error percentages”, except for a few data, is shown in Figure 5.18 for the data obtained from the experiments and Equation 5.2. Figure 5.18 reveals that about 70% of the data are within ±10% error lines while about 90% of the data are within ±30% error lines.

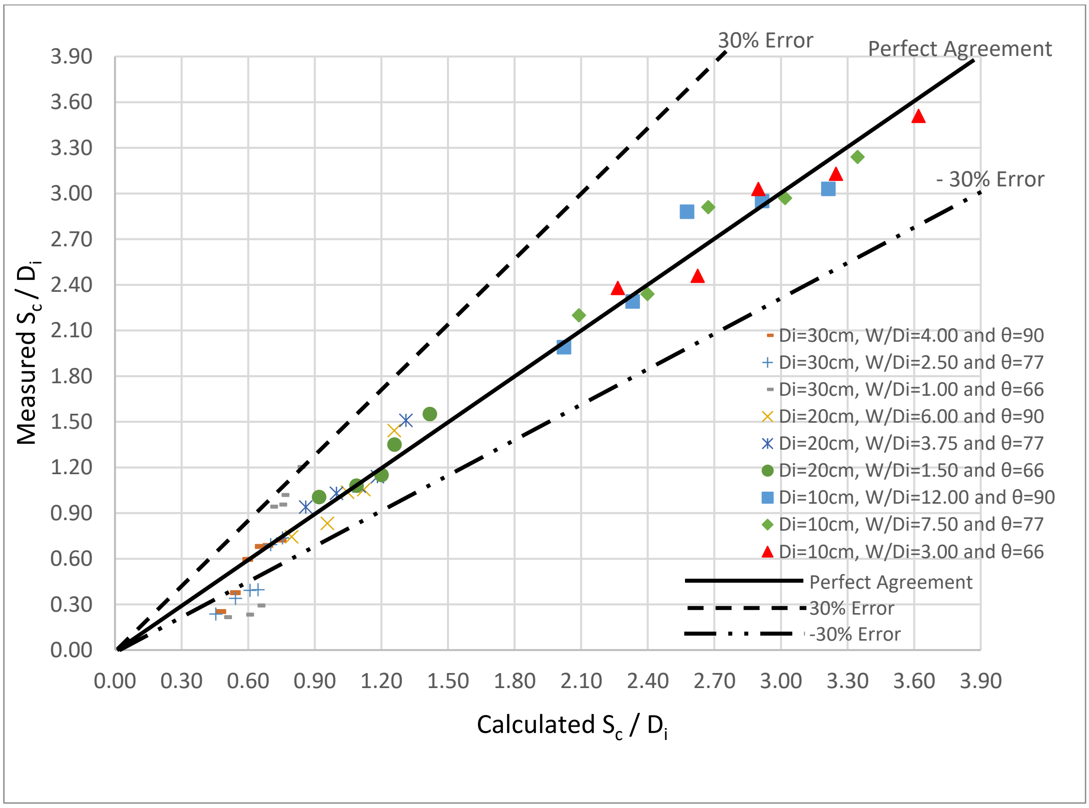

Figure 5.17 Comparison of The Measured S_c/D_i Data from Experimental Results and Calculated S_c/D_i Data from Equation 5.2

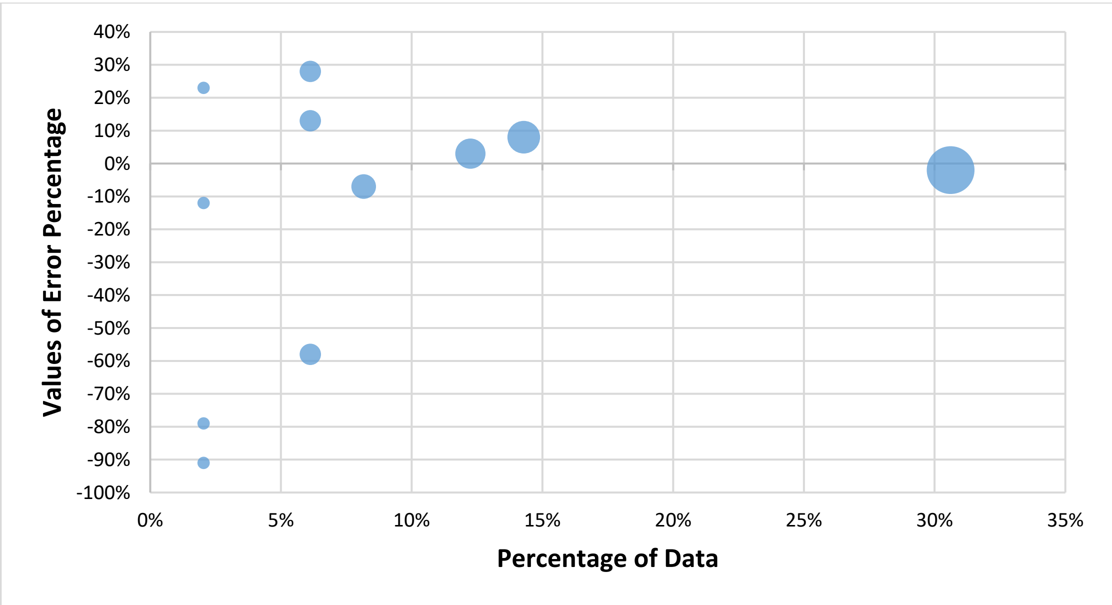

Figure 5.18 Relation between Parentage of data and Values of Error Percentage for Data Obtained from Experiment and Equation 5.2

5.5.2. Simplified Empirical Equations for S_c/D_i

Dimensionless terms of θ, W/D_i, We and Re were eliminated respectively from Equation 5.2 one by one assuming that their effect on S_c/D_i is negligible in order to obtain more simple empirical equations of S_c/D_i. Consequently, Equations 5.3, 5.4, 5.5 and 5.6 were derived by using regression analysis. These equations are valid for the limit values of dimensionless parameters expressed in Table 5.1.

$$\frac{S_c}{D_i} = \left(\frac{W}{D_i}\right)^{-0.089} Fr^{0.729} Re^{0.080} We^{-0.086} \tag{5.3}$$

with R^2=0.971

$$\frac{S_c}{D_i} = Fr^{0.609} Re^{0.008} We^{-0.008} \tag{5.4}$$

with R^2=0.963

$$\frac{S_c}{D_i} = Fr^{0.616} Re^{0.013} \tag{5.5}$$

with R^2=0.963

$$\frac{S_c}{D_i} = Fr^{0.722} \tag{5.6}$$

with R^2=0.942.

If the correlation coefficients, R^2, of the aforementioned equations are compared with each other, it is seen that they are slightly smaller than the general case which is indicated in Equation 5.2.

Figures 5.19, 5.21, 5.23 and 5.25 show comparison of the measured S_c/D_i data from experimental results and calculated S_c/D_i data from Equations 5.3, 5.4, 5.5 and 5.6, respectively with ±30% error lines. Figures 5.20, 5.22, 5.24 and 5.26 show variation of "parentage of data" with "values of error percentage" for the data obtained from the experiments and Equations 5.3, 5.4, 5.5 and 5.6, respectively. From the analysis of these figures it can be stated that the percentage of data within the error lines of ±30% varies from about 90% (Equation 5.3) to 80% (Equation 5.6) while those data within the error lines of ±10% varies from about 67% (Equation 5.3) to 30% (Equation 5.6).

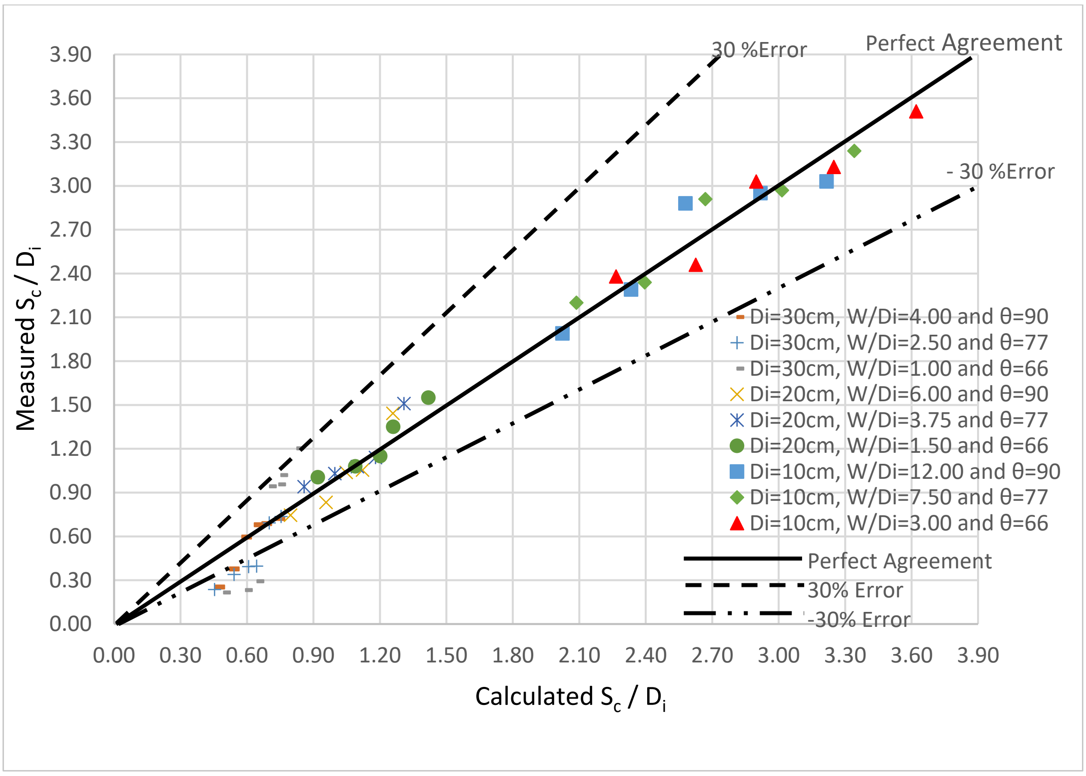

Figure 5.19 Comparison of The Measured Sc/Di Data from Experimental Results and Calculated Sc/Di Data from Equation 5.3

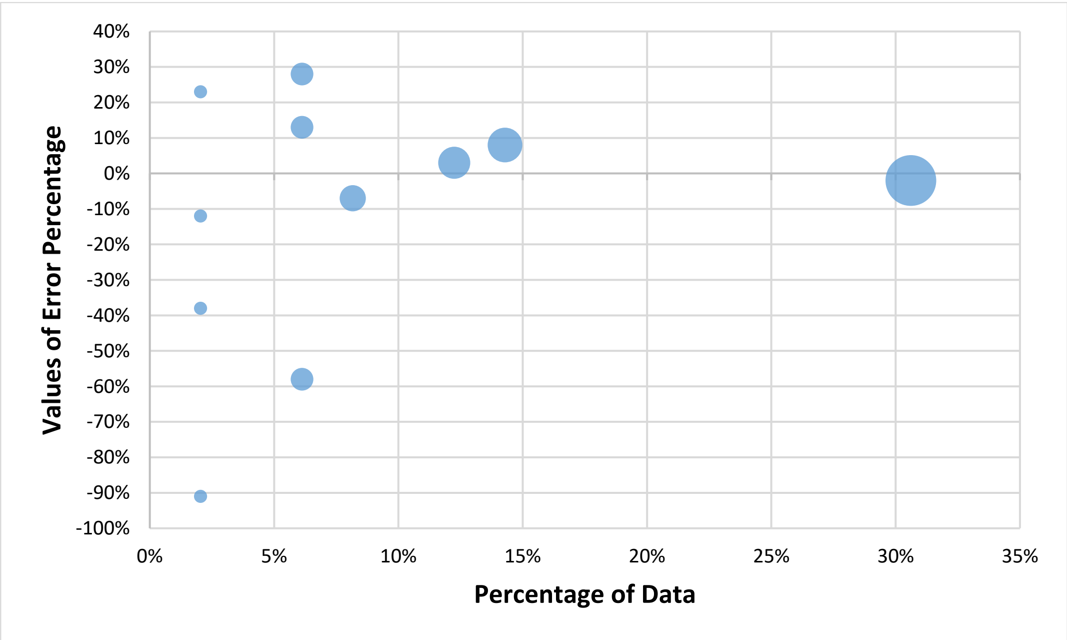

Figure 5.20 Relation between Parentage of data and Values of Error Percentage for Data Obtained from Experiment and Equation 5.3

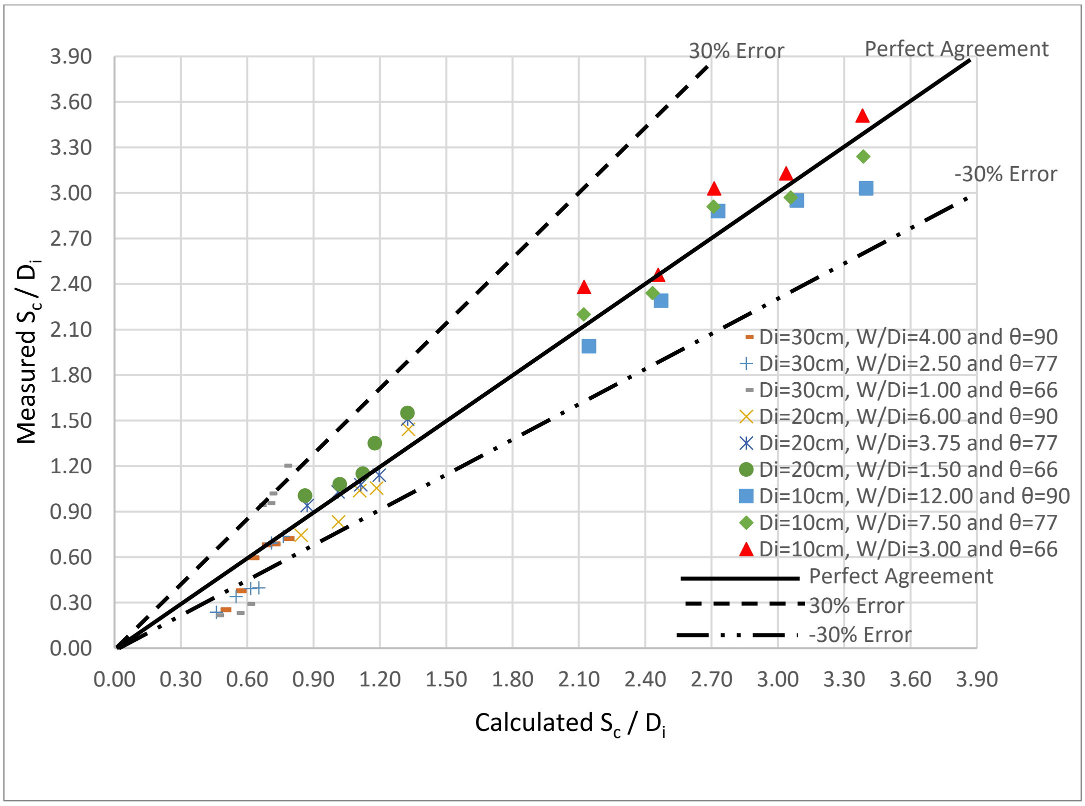

Figure 5.21 Comparison of The Measured Sc/Di Data from Experimental Results and Calculated Sc/Di Data from Equation 5.4

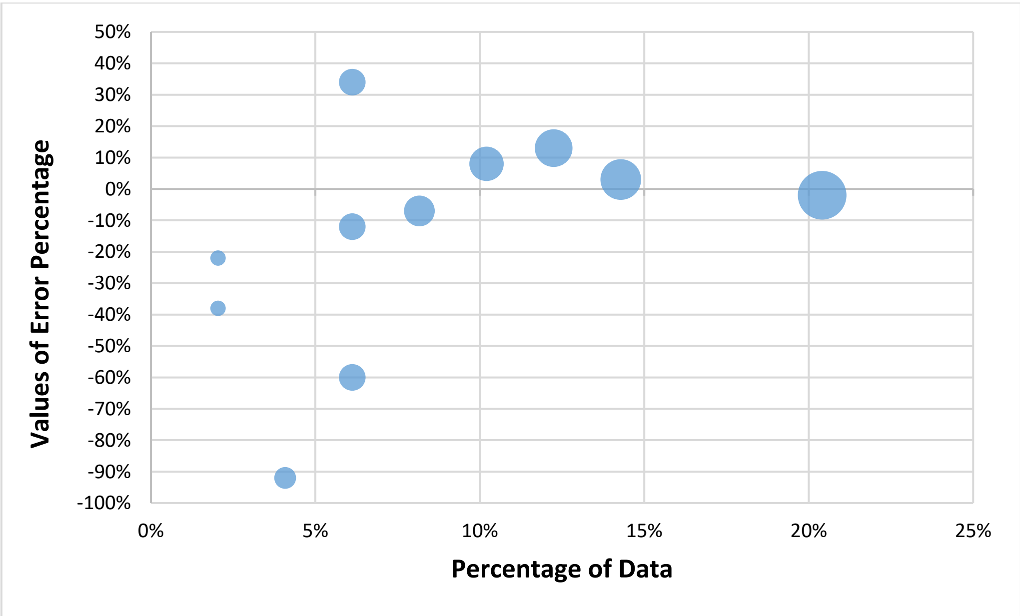

Figure 5.22 Relation between Parentage of data and Values of Error Percentage for Data Obtained from Experiment and Equation 5.4

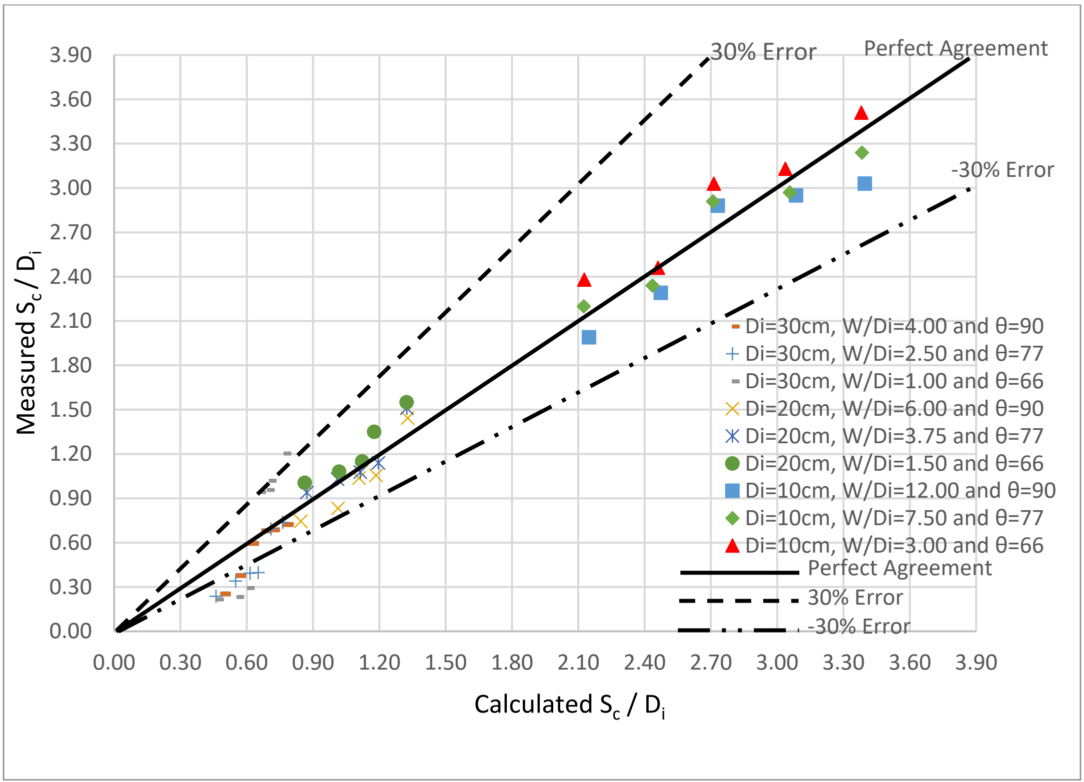

Figure 5.23 Comparison of The Measured Sc/Di Data from Experimental Results and Calculated Sc/Di Data from Equation 5.5

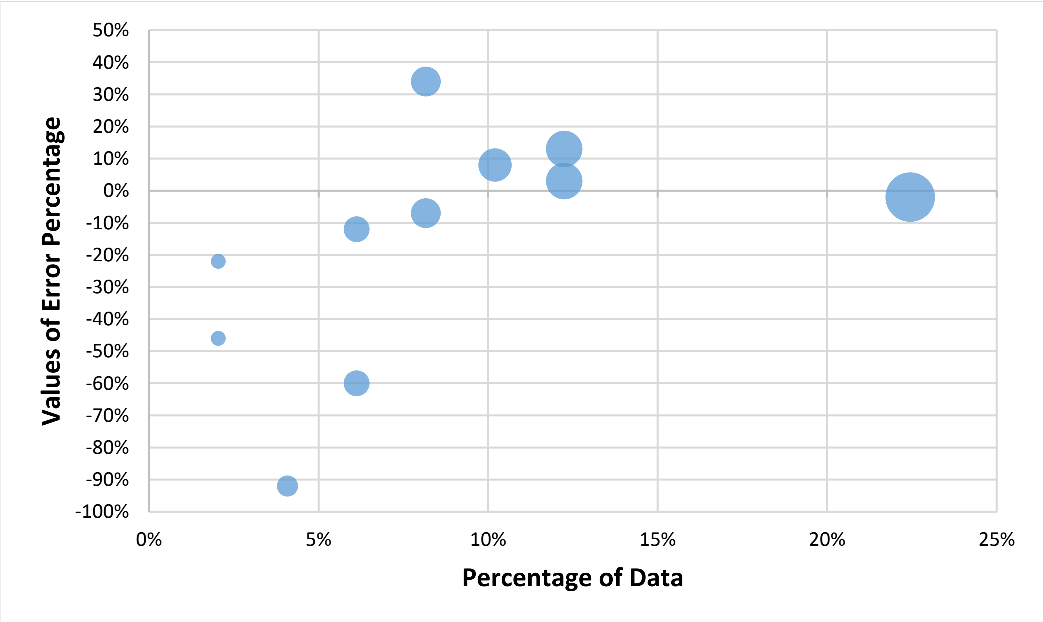

Figure 5.24 Relation between Parentage of data and Values of Error Percentage for Data Obtained from Experiment and Equation 5.5

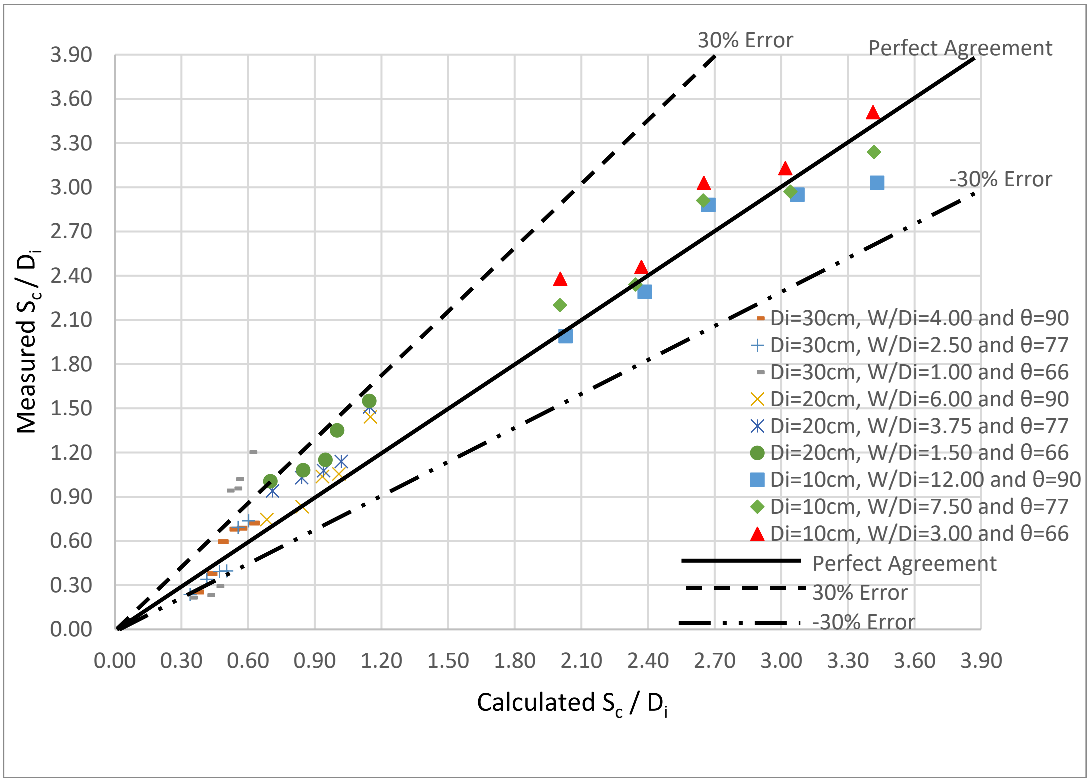

Figure 5.25 Comparison of The Measured Sc/Di Data from Experimental Results and Calculated Sc/Di Data from Equation 5.6

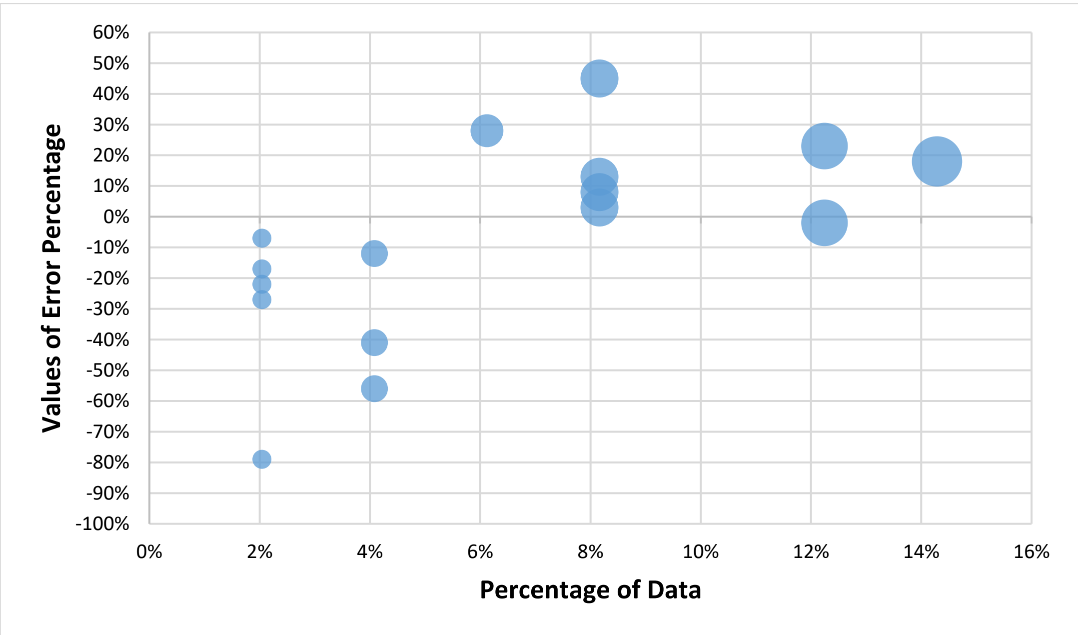

Figure 5.26 Relation between Parentage of data and Values of Error Percentage for Data Obtained from Experiment and Equation 5.6

5.6. Comparison of Present and Haspolat's (2015) Studies

Haspolat (2015) conducted similar study with the same experimental setup. As mentioned in the Chapter-2 (Literature Review), Haspolat estimated critical submergence for symmetrical approach channel flow conditions. Consequently, an empirical formula was derived to estimate critical submergence as a function of Fr,Re, We and $2b/D_i$ as indicated in Equation 2.13 ($S_c/D_i=Fr^{0.193}Re^{-0.331}We^{0.544}(2b/D_i)^{-0.241}$). In this equation, 2b is side wall clearance defined in Chapter 2.

Figure 5.27 shows a sketch of the side walls used in both studies. As it is seen from Figure 5.27, all the side wall angles, θ, used by Haspolat are 90° whereas side wall angles used in this study vary as a function of the side wall configurations tested (θ=90°, θ=77° and θ=66°). The distance between the right and left approach channel side walls along the head wall of the intake (W) for the present study is equal to the sidewall clearance (2b) used by Haspolat. Therefore, the values of W/D_i and $2b/D_i$ are the same as indicated in Figure 5.27. Figure 5.27 also shows the dead zones for the both studies which are designated by (1), (2) and (3).

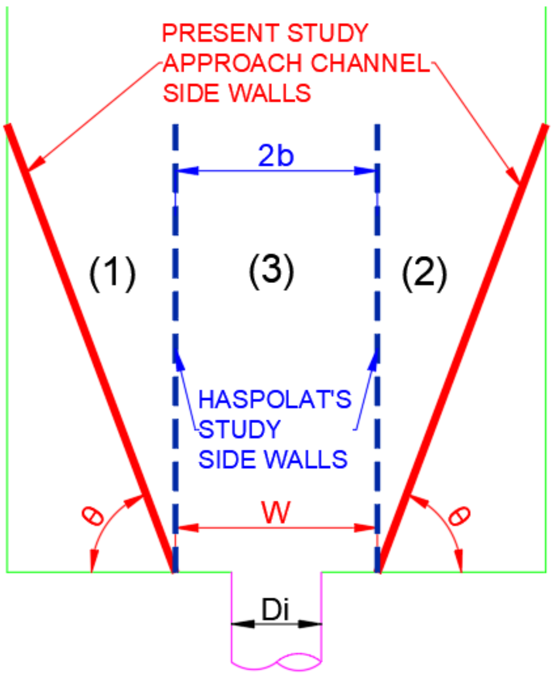

Figure 5.27 Sketch Showing the Approach Channel Walls Used in the Present and Haspolat's Studies

Since the present experimental setup contains different side walls angles, θ, two different empirical equation of present study was used in the comparison. Equation 5.2 ($S_c/D_i = (W/D_i)^{-0.081} Fr^{0.718} Re^{0.075} We^{-0.078} \theta^{-0.038}$) and Equation 5.3 ($S_c/D_i = (W/D_i)^{-0.089} Fr^{0.729} Re^{0.080} We^{-0.086}$), belonging to the present study, was used for the comparison. Equation 5.2 regards effect of θ whereas Equation 5.3 ignores effect of θ.

When the side wall angles are 90^o, both studies consist of dead zone of only (3). In this case, all the geometric properties are the same for both studies. Present and Haspolat's studies were compared with each other in terms of S_c/D_i values obtained by using the empirical equations of S_c/D_i derived from the both studies for the experimental data of the present study (Figure 5.28); Equation 2.13(Haspolat) and Equation 5.3(present study). As it can be seen from Figure 5.28, all the data are within the error lines of ±15% except a couple of data. From this figure one can say that there is a good agreement between the both empirical equations used here to estimate the value of S_c/D_i.

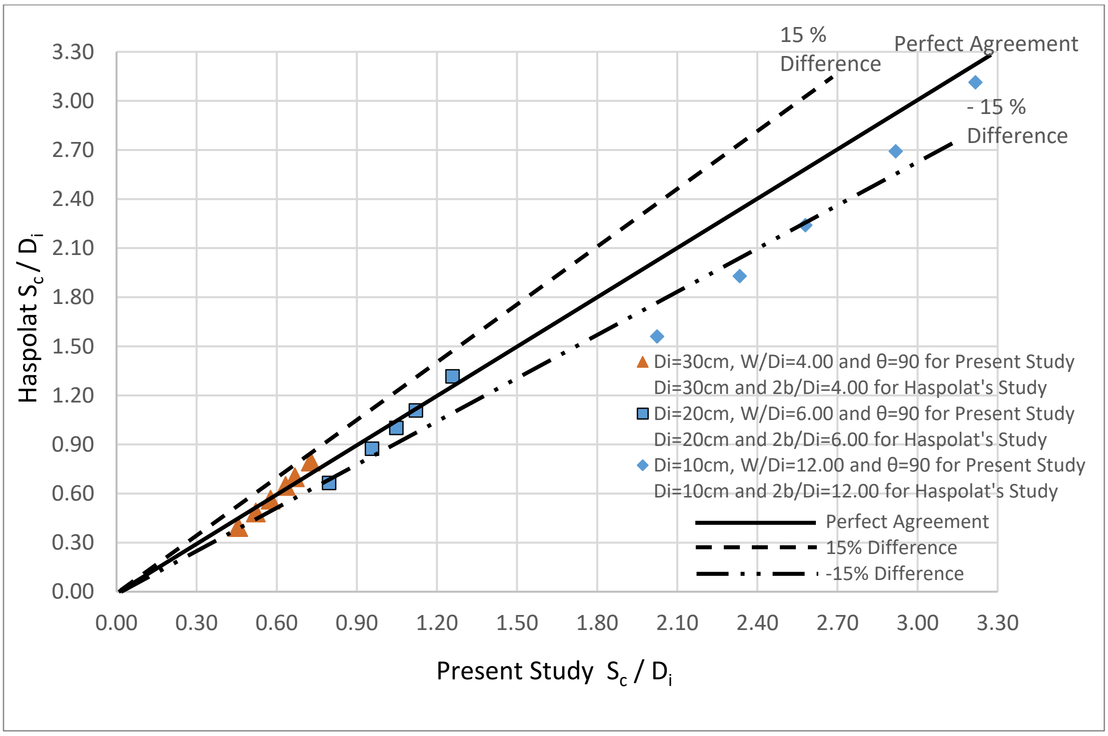

Figure 5.28 Comparison of the Calculated S_c/D_i values from Haspolat's Relationship (Equation 2.13) and Present Study (Equation 5.3) for the case of θ=90°

When side wall angles, θ, are 77° and 66°, the present study consists of dead zones of (1), (2) and (3) whereas Haspolat's study has dead zone of only (3). In this case, the approach flow geometric properties are different for the both studies. Therefore, in this case Equation 5.2 for the present study and Equation 2.13 for Haspolat's study were compared with each other using the present study data (Figure 5.29). The side wall angles used in the derivation of Equation 2.13 in Haspolat's study are all 90° whereas the experimental data of the present study was obtained with approach channel side walls having different θ values. Therefore, as Figure 5.29 prevails, all the data points appear within the error lines ±25%. From the analysis of Figure 5.29 it can be stated that especially at small values of W/D_i (or $2b/D_i$); 1.0, 1.5, 2.5 and 3.75, Equation 2.13 estimates larger values than those of Equation 5.2. The reason of this situation can be explained as follows: as the value of W/D_i gets smaller the effect of boundary blockage on the value of S_c/D_i increases and therefore, S_c/D_i values are observed at larger submergence. As the value of W/D_i gets larger than about 3.75, the agreement between Equation 2.13 and 5.2 becomes much better.

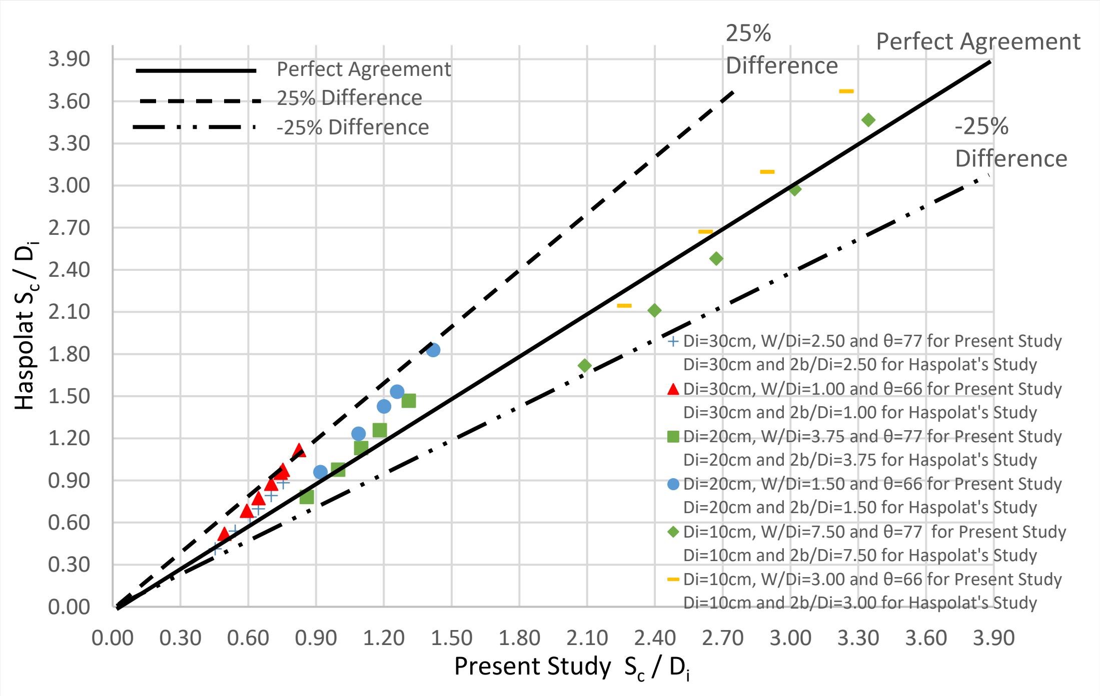

Figure 5.29 Comparison of the Calculated S_c/D_i values from Haspolat's Relationship (Equation 2.13) and Present Study (Equation 5.2) for the case of θ=66º and θ=77º

CHAPTER 6

CONCLUSIONS AND RECOMMENDATIONS

In the present study, formation of air-entraining vortices was investigated in a physical model for different symmetrical approach channel configurations. Series of experiments were performed with various discharges and intake pipe diameters. Consequently, the critical submergence was observed for each experiment. Empirical formulas related with the hydraulic and flow parameters were derived to estimate critical submergence. Simplified empirical equations were also obtained from general form of the empirical equations. The following conclusions can be drawn from the results of this study.

1. Increase in dimensionless parameters of Fr, Re and We causes increasing of S_c/D_i values for all the approach channel configurations tested.

2. For a given constant Fr, Re or We, S_c/D_i values tend to increase with the decrease of W/D_i as indicated in Figures 5.4-5.12. Also, it can be stated that effect of W/D_i on critical submergence may be accepted as negligible if W/D_i values start to exceed 6 as stated by Gürbüzdal (2009).

3. The experimental setups having the approach channel side walls perpendicular to the intake head wall, $\theta=90^o$ give almost all the time minimum S_c/D_i values compared to those of $\theta=66^o$ and $\theta=77^o$.

4. Empirical equations were derived to obtain critical submergence from dimensionless parameters of S_c/D_i, W/D_i and θ for a given Fr, Re and We with high correlation coefficients.

5. Eliminating some of the dimensionless terms, Re, We, W/D_i and θ, from the general empirical equation of S_c/D_i (Equation 3.5) do not affect the critical submergence significantly.

The following recommendations can be presented for future studies:

1. Similar studies can be performed with the same approach flow conditions by using intake pipes of different diameters.

2. A large scale model of the experimental setup can be used to repeat the study to get information for the effect of scale effect on the values of S_c/Di.

REFERENCES

Anwar, H.O. (1967), “Vortices at Low Head Intakes”, Water Power 1967(11), 455 457.

Anwar, H.O. (1968), “Prevention of Vortices at Intakes”, Water Power 1968(10), 393-401.

Anwar, H.O., Weller, J.A. and Amphlett, M.B. (1978), “Similarity of Free-Vortex at Horizontal Intake”, J. Hydraulic Res. 1978(2), 95-105.

Baykara, A., (2013), “Effect of Hydraulic Parameters on the Formation of Vortices at Intake Structures”, M.S. Thesis, Civil Engineering Dept., METU.

Daggett, L.L. and Keulegan, G.H. (1974), “Similitude in Free-Surface Vortex Formations”, J. Hydraulic Div., ASCE, HY11, 1565-1581.

Durgin, W.W. and Hecker, G.E. (1978), The Modeling of Vortices in Intake Structures. Proc IAHR-ASME-ASCE Joint Symposium on Design and Operation of Fluid Machinery, CSU Fort Collins, June 1978 vols I and III.

Gordon, J.L. (1970), “Vortices at Intakes”, Water Power 1970(4), 137-138.

Gulliver, J.S. and Rindels, A.J. (1983), “An Experimental Study of Critical Submergence to Avoid Free-surface Vortices at Vertical Intakes”, Project Report No: 224, University of Minnesota, St. Anthony Falls Hydraulic Laboratory.

Gogus, M., Koken, M. and Baykara A. (2016), “Formation of Air-entraining Vortices at Horizontal Intakes without Approach Flow Induced Circulation”, Journal of Hydromechanics, Science Direct, 28(1), 102-113.

Gürbüzdal, F., (2009), “Scale effects on the formation of vortices at intake structures”, M.S. Thesis, Civil Engineering Dept., METU.

Haspolat, E., (2009), “Determination of Critical Submergence Depth at Horizontal Intakes”, M.S. Thesis, Civil Engineering Dept., METU.

Hecker, G.E. (1981) “Model- Prototype Comparision of Free Surface Vortices”, J.Hydraulic Div., ASCE, HY10, 1243-1259.

Jain, A.K., Kittur, G.R.R., and Ramanchandra, J.G. (1978), “Vortex Formation at Vertical Pipe Intakes”, J. Hydraulic Div., ASCE, HY10, 1429-1448.

Jiming, M., Yuanbo, L. and Jitang, H. (2000), “Minimum Submergence before Double- Entrance Pressure Intakes”, J. Hydraulic Div., ASCE, HY10, 628-631

Knauss, J. (1987), “Swirling Flow Problems at Intakes”, A.A. Balkema, Rotterdam.

Oakdale Engineering web site, http://www.oakdaleengr.com/download.htm, last accessed on 16.05.2019

Padmanabhan, M. and Hecker, G.E. (1984), “Scale Effects in Pump Sump Models”, J. Hydraulic Engineering, ASCE, 110, HY11, 1540-1556.

Reddy, Y.R. and Pickford, J.A. (1972), “Vortices at Intakes in Conventional Sumps”, Water Power 1972(3), 108-109.

Sarkardeh H., Zarrati A.R. and Roshan R. (2010) “Effect of intake head wall and trash rack on vortices”, J. Hydraulic Research, 48:1, 108-112

Taştan, K. and Yıldırım, N. (2010), “Effects of Dimensionless Parameters on Air-entraining Vortices”, J. Hydraulic Research, 48:1, 57-64.

Taştan, K. and Yıldırım, N. (2014), “Effects of Froude, Reynolds, and Weber numbers on an air- entraining vortex”, J. Hydraulic Research, 52:3, 421-425.

Yıldırım, N. and Kocabaş, F. (1995), “Critical Submergence for Intakes in Open Channel Flow”, J. Hydraulic Engng., ASCE, 121, HY12, 900-905.

Yıldırım, N., Kocabaş, F. and Gülcan, S.C (2000), “Flow-Boundary Effects on Critical Submergence of Intake Pipe”, J. Hydraulic Engng., ASCE, 126, HY4, 288-297.

Yıldırım, N., Taştan, K. and Arslan, M.M. (2009) “Critical Submergence for Dual Pipe Intakes”, J. Hydraulic Research, 47:2, 242-249.

Zaloğlu, C., (2014), “Formation of Air Entraining Vortices at Horizontal Water Intakes”, M.S. Thesis, Civil Engineering Dept., METU.

Zeigler, E.R. (1976), “Hydraulic Model Vortex Study Grand Coulee Third Powerplant”, Engineering and Research Center, U.S Bureau of Reclamation, Denver, Colorado.

APPENDICES

A. Experimental Results

In this part, experimental results are shown in tabular from. In these tables discharge, critical submergence and the related dimensionless parameters are presented. The main geometrical properties with intake velocity and discharge are shown in the Figure A.1.

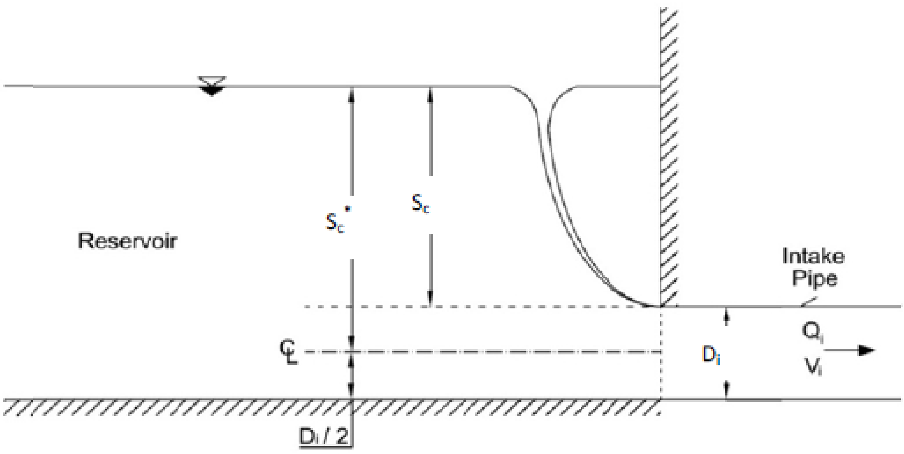

Figure A.1 Simple Sketch of the Main Geometrical Properties with Intake Velocity and Discharge

Physical properties of water, which are used to obtain the flow parameters such as Froude, Reynolds and Weber numbers, are taken as;

$g = 9.81\ m/s^2$

$\nu = 1.004 \times 10^{-6}\ m^2/s$

$\sigma = 7.28 \times 10^{-2}\ N/m$

$\rho = 998\ kg/m^3$

Table A.1 *Experimental results of critical submergence and related important flow parameters for D_i=30cm, W/D_i=4.00, L/D_i=3.33 and θ=90^0*

Obs	Qi(lt/s)	Sc (cm)	Sc/Di	V(m/s)	Fr	Re	We
1	60.75	21.65	0.722	0.859	0.501	256816	3038
2	53.07	20.60	0.687	0.751	0.438	224326	2318
3	48.86	20.40	0.680	0.691	0.403	206546	1965
4	42.17	17.85	0.595	0.597	0.348	178268	1464
5	36.01	11.30	0.377	0.509	0.297	152222	1067
6	29.15	7.60	0.253	0.412	0.240	123207	699

Table A.2 *Experimental results of critical submergence and related important flow parameters for D_i=30cm, W/D_i=2.50, L/D_i=3.43 and θ=77^0*

Obs	Qi(lt/s)	Sc (cm)	Sc/Di	V(m/s)	Fr	Re	We
1	60.128	22.10	0.737	0.851	0.496	254174	2976
2	53.640	20.80	0.693	0.759	0.442	226748	2368
3	46.900	11.90	0.397	0.663	0.387	198257	1811
4	42.788	11.80	0.393	0.605	0.353	180874	1507
5	35.715	10.20	0.340	0.505	0.295	150975	1050
6	26.983	7.10	0.237	0.382	0.223	114063	599

Table A.3 *Experimental results of critical submergence and related important flow parameters for D_i=30cm, W/D_i=1.00, L/D_i=3.67 and θ=66^0*

Obs	Qi(lt/s)	Sc (cm)	Sc/Di	V(m/s)	Fr	Re	We
1	61.002	36.10	1.203	0.863	0.503	257869	3063
2	52.903	30.60	1.020	0.748	0.436	223633	2304
3	51.769	28.70	0.957	0.732	0.427	218837	2206
4	47.244	28.30	0.943	0.668	0.390	199711	1837
5	41.490	8.80	0.293	0.587	0.342	175385	1417
6	36.418	7.00	0.233	0.515	0.300	153947	1092
7	27.300	6.50	0.217	0.386	0.225	115403	613

Table A.4 *Experimental results of critical submergence and related important flow parameters for D_i=20cm, W/D_i=6.00, L/D_i=5.00 and* $\theta=90^0$

Obs	Qi(lt/s)	Sc (cm)	Sc/Di	V(m/s)	Fr	Re	We
1	53.382	28.85	1.443	1.699	1.213	338486	7916
2	44.517	21.10	1.055	1.417	1.012	282275	5505
3	40.053	20.75	1.038	1.275	0.910	253966	4456
4	34.710	16.65	0.833	1.105	0.789	220090	3347
5	25.998	14.90	0.745	0.828	0.591	164846	1878

Table A.5 *Experimental results of critical submergence and related important flow parameters for D_i=20cm, W/D_i=3.75, L/D_i=5.15 and* $\theta=77^0$

Obs	Qi(lt/s)	Sc (cm)	Sc/Di	V(m/s)	Fr	Re	We
1	53.145	30.20	1.510	1.692	1.208	336984	7846
2	45.191	22.80	1.140	1.438	1.027	286549	5673
3	40.365	21.55	1.078	1.285	0.917	255945	4526
4	34.615	20.60	1.030	1.102	0.787	219488	3329
5	27.378	18.80	0.940	0.871	0.622	173599	2082

*Tab*le A.6 *Experimental results of critical submergence and related important flow parameters for D_i=20cm, W/D_i=1.50, L/D_i=5.50 and* $\theta=66^0$

Obs	Qi(lt/s)	Sc (cm)	Sc/Di	V(m/s)	Fr	Re	We
1	53.102	31.00	1.550	1.690	1.207	336711	7833
2	44.059	27.00	1.350	1.402	1.001	279371	5393
3	40.887	23.00	1.150	1.301	0.929	259258	4644
4	35.036	21.60	1.080	1.115	0.796	222157	3410
5	26.895	20.10	1.005	0.856	0.611	170537	2009

Table A.7 *Experimental results of critical submergence and related important flow parameters for D_i=10cm, W/D_i=12.00, L/D_i=10.0 and θ=90^0*

Obs	Qi(lt/s)	Sc (cm)	Sc/Di	V(m/s)	Fr	Re	We
1	42.897	30.30	3.030	5.462	5.514	544006	40895
2	36.807	29.50	2.950	4.686	4.732	466774	30108
3	30.332	28.80	2.880	3.862	3.899	384660	20447
4	25.916	22.90	2.290	3.300	3.332	328658	14926
5	20.726	19.90	1.990	2.639	2.664	262834	9546

Table A.8 Experimental results of critical submergence and related important flow parameters for D_i=10cm, W/D_i=7.50, L/D_i=10.3 and θ=77^0

Obs	Qi(lt/s)	Sc (cm)	Sc/Di	V(m/s)	Fr	Re	We
1	42.637	32.40	3.240	5.429	5.481	540708	40401
2	36.278	29.70	2.970	4.619	4.664	460066	29249
3	29.956	29.10	2.910	3.814	3.851	379892	19943
4	25.280	23.40	2.340	3.219	3.250	320593	14203
5	20.359	22.00	2.200	2.592	2.617	258186	9212

Table A.9 *Experimental results of critical submergence and related important flow parameters for Di=10cm, W/Di=3.00, L/Di=11.0 and θ=66^0*

Obs	Qi(lt/s)	Sc (cm)	Sc/Di	V(m/s)	Fr	Re	We
1	42.563	35.10	3.510	5.419	5.472	539770	40261
2	35.897	31.30	3.130	4.571	4.615	455234	28638
3	30.010	30.30	3.030	3.821	3.858	380577	20015
4	25.691	24.60	2.460	3.271	3.303	325805	14668
5	20.383	23.80	2.380	2.595	2.620	258490	9233